Zhang *et al. Energy Mater* 2023;3:300022
DOI: 10.20517/energymater.2023.06

Energy Materials

Review

Open Access

Check for updates

Recent advances in the type, synthesis and electrochemical application of defective metal-organic frameworks

Yanfei Zhang[#], Qian Li[#], Guangxun Zhang, Tingting Lv, Pengbiao Geng, Yumeng Chen, Huan Pang[*]

School of Chemistry and Chemical Engineering, Yangzhou University, Yangzhou 225009, Jiangsu, China.
[#]Authors contributed equally.

***Correspondence to:** Prof. Huan Pang, School of Chemistry and Chemical Engineering, Yangzhou University, Yangzhou 225009, Jiangsu, China. E-mail: panghuan@yzu.edu.cn or huanpangchem@hotmail.com

How to cite this article: Zhang Y, Li Q, Zhang G, Lv T, Geng P, Chen Y, Pang H. Recent advances in the type, synthesis and electrochemical application of defective metal-organic frameworks. *Energy Mater* 2023;3:300022. https://dx.doi.org/10.20517/energymater.2023.06

Received: 7 Feb 2023 **First Decision:** 7 Mar 2023 **Revised:** 11 Mar 2023 **Accepted:** 11 Apr 2023 **Published:** 12 May 2023

Academic Editor: Yuhui Chen **Copy Editor:** Fangling Lan **Production Editor:** Fangling Lan

Abstract

Metal-organic frameworks (MOFs) have attracted increasing attention in electrochemistry due to their inherent characteristics, such as large specific surface area, high porosity, and structural flexibility. Defects can be designed and generated during the synthesis of MOFs, and their presence gives MOF materials excellent properties in terms of electrochemical energy conversion and storage. This review focuses on the types of defects in MOFs and presents recent and important advances in the methods for introducing defects into MOFs and the effects of defects on the physicochemical properties of MOFs, with emphasis on the application of defective MOFs as catalysts for electrochemical energy conversion and storage. On this basis, the current advantages and disadvantages of defective MOFs in electrochemical energy conversion and storage are presented and future research directions for defective MOFs construction in electrochemical applications are proposed.

Keywords: Metal-organic framework, defects, vacancy, catalyst, electrochemical

INTRODUCTION

With the continuous development of the global economy, the continuous use of fossil fuels has caused environmental damage and a lack of resources, which constantly urges researchers to explore new

technologies of green, environmental protection and renewable energy[1-3]. Currently, many renewable energy technologies are gradually replacing fossil fuels[4-6]. Among them, electrochemical energy conversion and storage technology are considered as one of the most promising clean and sustainable energy technologies[7-11]. Electrocatalytic energy conversion, such as oxygen evolution reaction (OER)[12-16], oxygen reduction reaction (ORR)[17-19], hydrogen evolution reaction (HER)[20-22], and CO_2 reduction reaction (CO_2RR)[23,24], and electrochemical energy storage, the use of devices such as Lithium-ion batteries (LIBs)[25-29], Zinc-ion batteries (ZIBs)[30-33], Lithium-sulfur batteries (LI-S)[34-42], Supercapacitors (SCs)[43-45], and other batteries[46-48] are all critical factors in the development of renewable energy. In addition, both depend largely on the electrocatalyst and electrode materials in practical applications. Consequently, the reasonable design and preparation of electrocatalysts and electrode materials with the required properties are essential in developing electrochemical energy conversion/storage technologies[49,50].

As a novel class of porous materials, MOFs are widely used in gas separation[51,52], substrates for drug delivery[53], chemical sensing[54-56], catalysis[57,58], and biosensors[59,60] due to their unique properties (processability, structural flexibility, and high specific surface area). Compared to conventional porous materials (activated carbon, mesoporous silica, zeolite, *etc.*), MOFs can provide appropriate space for electrochemical reactions and ion storage/transfer due to their high surface area[61-63]. As a result, the application of MOFs in electrocatalytic energy conversion and electrochemical energy storage has attracted the attention of more and more researchers. However, the vast majority of MOFs have poor conductivity ($< 10^{-10}$ S·cm^{-1}), which greatly limits their application in electrochemistry[64,65]. For most MOFs with poor electrochemical performance, the pore size and shape of the framework can be artificially modulated inside the MOFs by elimination reactions in advance to enhance charge and mass migration. In the past decade, most studies have shown that the presence of defects in MOFs has been proven to be effective in altering the periodic crystal structure and affecting the surrounding charge distribution, improving the physicochemical properties of the electrode materials and thus expanding the MOFs applications[66-68]. Nevertheless, researchers are still committed to improving the electrochemical performance of MOFs to create the perfect electrode materials.

The smart control of property-affecting defects and the arrangement of these defects in the crystalline microporous materials (i.e., microcosmic structure) makes it possible to achieve functionality-specific "defect engineering" in MOFs[69]. To date, researchers have designed and synthesized tens of thousands of MOFs. Still, few of these MOFs are flawless because any small change in reaction conditions can lead to vacancies or defects in the MOFs framework, resulting in defective MOFs. The corresponding publications in recent years are summarized in Figure 1. Defects in MOFs can be the missing of metal centers, the missing of organic ligands, as well as the doping of defective or functionalized ligands, *etc.*[70], which means that the original periodic structure of the framework is disrupted. However, in some specific cases, defects can enhance MOFs' performance by altering their surface properties and internal pore structure or exposing active metal sites[71,72], such as gas storage, gas separation and catalytic[73] properties. Meanwhile, advanced preparation technologies and mature characterization methods have greatly accelerated the development of defects in MOFs, such as plasma etching, pyrolysis treatment and electron diffraction, which can deeply explore the applications of defects in the electrochemical aspects[5,74,75]. In recent years, defective materials of MOFs have been summarized in many review articles. Compared with non-defective MOFs, defective MOFs have outstanding electrochemical performance and excellent structural stability with promising potential for electrochemical applications[76]. Therefore, it is necessary to comprehensively and systematically summarize the electrochemical applications of defective materials of MOFs.

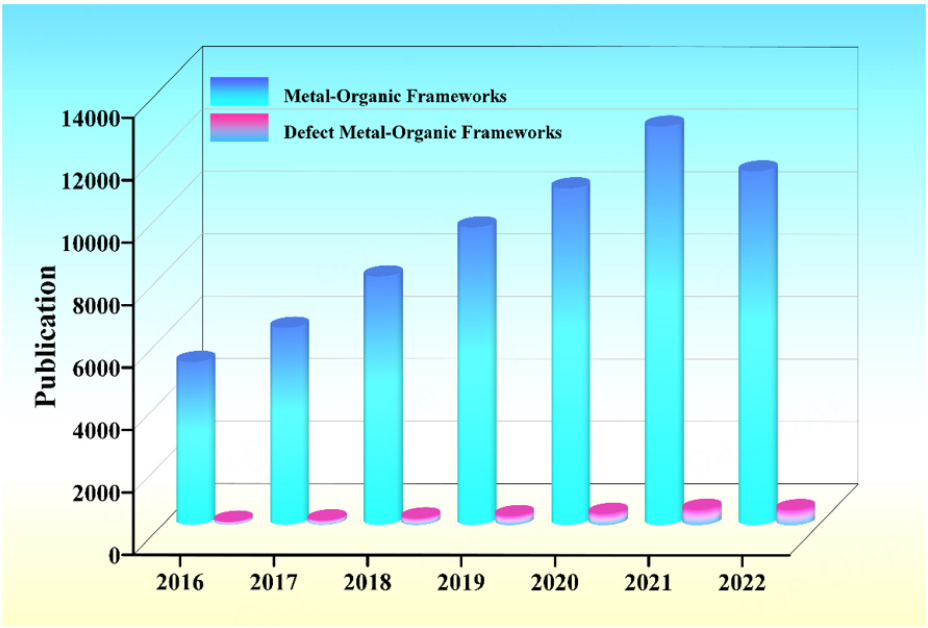

Figure 1. The total number of publications on MOFs/defect MOFs in the past few years (2016-2022), as searched in "Web of Science".

The excellent properties of defective MOFs make them ideal materials for electrochemical applications, and researchers are constantly working to prepare novel defective MOFs with the desired properties. Therefore, numerous reviews focusing on the synthesis and applications of defective MOFs have been published. For instance, Zhong *et al.* reported the application of defective MOFs to nitrogen reduction reactions[23]. Fang *et al.* present the emerging research field of defect-engineered MOFs and coordination network compounds in a systematic fashion[74]. Zhu *et al.* review recent advances in MOF as an electrocatalyst in the field of electrochemical CO_2 reduction and outline critical insights into the structure-performance relationship and performance adjustment[57]. Similarly, Narváez-Celada *et al.* have systematically reviewed the application of MOFs as catalysts for electrochemical CO_2 reduction reactions[58]. More detail, Pang's review has concentrated on the formation, arrangement, and functions of MOF defects[69]. Hence, the recent progress of defective MOFs and their derivatives for electrocatalysis composed of HER, OER and ORR have been concluded in Wu's report[23]. Although there have been many reviews in this research field, the review on the application of defective MOFs in electrochemical energy storage and electrochemistry is still not very detailed. We first review the different types of defective MOFs and the characteristics of the different defect types are analyzed. Then the preparation strategies of defective MOFs are highlighted, and the advantages and disadvantages of different preparation strategies are detailed [Figure 2], as well as the recent research progress of defective MOFs in energy conversion and storage applications, which are obviously different from other reviews. Finally, the key challenges of defective MOFs in electrochemistry are proposed, and some relevant ideas for future research are put forward. We hope that the present review will benefit the readers to rationally design and develop defective MOFs for electrochemical applications.

TYPES OF DEFECTS IN MOFS

Defects of diverse properties and molecular length scales are important attributes of MOFs, and knowledge of the defect structure of a material can enable better application of its performance[77,78]. Based on the composition and size of the missing fragments in the structure, the types of defects in MOFs were classified into three categories, namely linker defects, cluster defects, and macroscopic defects [Table 1].

Table 1. The relevant publications on the types of defective MOFs

Compound	Type of defect(s)	Characterization	Applications	Reference
ZnBLD MOFs	Missing linkers	FTIR, TGA, ^{1}H NMR, ICP and PXRD	The chiral separation capacity	[79]
Uio-66	Missing linkers	High-resolution neutron powder diffraction	Gas adsorption	[80]
Zr-MOFs	Missing linkers	PXRD, SCXRD, UV, TEM, IR, SEM, MS	Guest adsorption and catalytic performance	[82]
CoBDC	Missing linkers	TEM, SEM, synchrotron X-ray	OER	[83]
Uio-66	Missing linkers	PXRD, TGA	Conductivity	[84]
MOF-808	Missing linkers	PXRD, TGA, XPS	Conductivity	[85]
Uio-66	Missing clusters	XRD, TGA	Catalysis	[88]
Uio-66	Missing clusters	PXRD, TGA, electron microscopy, anomalous X-ray scattering	-	[93]
Uio-66	Missing clusters	^{1}H NMR, BET, Ex situ characterization	CO_2 sorption	[94]
Uio-66	Missing clusters	PXRD, N_2 sorption, dissolution/NMR, TGA-DSC, SEM/EDX, and ATR-IR	-	[95]
Uio-66	Missing linkers/clusters	PXRD, HRTEM, ^{13}C NMR	Catalysis	[73]
Uio-66	Missing linkers/clusters	XRD, SEM, UV, BET, TGA	Nitrogen fixation photocatalysts	[96]
HKUST-1	Missing linkers/paddlewheels	PXRD, SEM, IR, TGA, NMR and N_2 sorption	-	[99]
MOF-5	Macroscopic	PXRD, HRTEM, TEM, SEM	Gas adsorption and catalysis	[100]
MIL-100 (Fe)	Macroscopic	PXRD, XPS, TEM, SEM, HRTEM, EDS	-	[101]
Uio-66	Macroscopic	PXRD, XRD, TEM, SEM	Protein delivery	[103]
MOF-5	Macroscopic	PXRD, TEM, SEM	CO_2 adsorption	[104]
Uio-66	Macroscopic	PXRD, TEM, BET	Catalysis	[105]

Missing linker defects

A comprehensive understanding of structural defects is a critical step in the rational design of defect engineering MOFs (DEMOFs). Owing to the high design flexibility of MOFs, the missing linkers can be controllably introduced into MOFs by partially substituting multi-coordinating bridging linkers with nonbridging ligands to change their coordination environment without loss of crystallinity and porosity of materials. So, incorporating missing linkers into MOFs provides a promising strategy to tailor electronic structure of MOFs[79,80]. The introduction of missing linkers in the structure of MOFs may open up new opportunities for regulating the performance of MOFs[81].

Yuan *et al.* proposed a method to predictably increase the porosity and pore size of microporous MOFs inspired by a combination of linker installation, and solvent-assisted ligand approaches[82]. The above method utilizes MOFs with coordination bond unsaturated $Zr_6O_4(OH)_8(H_2O)_4$ clusters and post-synthetically replaces the terminal -OH /H_2O on the Zr_6 cluster by carboxylates. The reverse of linker installation can lead to the formation of linker labilization, and under acidic conditions, the pro-labile linker can cleave into two removable carboxylates, introducing defects [Figure 3A]. The maximum pore size can be regulated from 1.5~18 nm as determined by N_2 sorption analysis using a reasonable adjustment of the pro-labile linker content and acid concentration during linker labilization process during MOFs synthesis. Linker labilization allows the selective preparation of porous structures with different porosity levels, prompting the guest's rapid diffusion throughout the framework, making them attractive as one of the most prodigious materials for applications, including adsorption and electrochemistry.

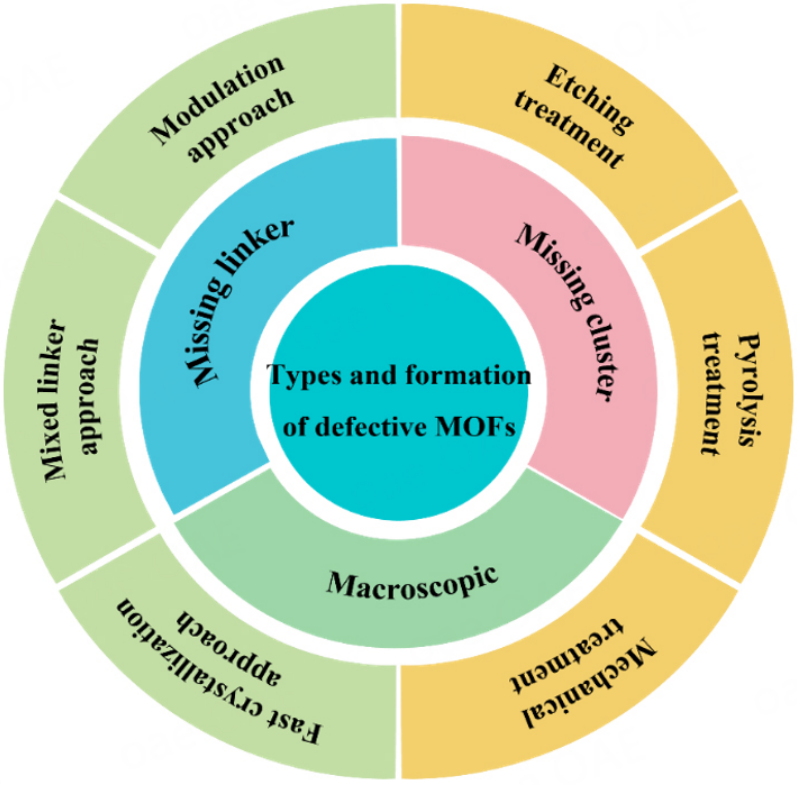

Figure 2. Schematic diagram of the main synthesis strategies and types of defective MOFs.

Moreover, it will provide a promising strategy for tailoring the electronic structure of MOFs by introducing missing linkers in the structure of MOFs, thus creating new opportunities for improving the electrocatalytic performance of MOFs[81]. Xue and his coworkers[83] proposed that the incorporation of the missing linker into the MOFs could effectively improve the electrocatalytic performance. DFT calculations revealed that the electronic structure of MOFs can be modulated by the introduction of missing linkers, thus increasing the OER activity of MOFs [Figure 3B]. The introduction of the missing linker resulted in the formation of new electronic states near the Fermi level, which implied that the tuning of the electronic structure of CoBDC-Fc made it excellent for OER performance [Figure 3C]. The analysis based on the free energy diagram of CoBDC [Figure 3D] revealed that the energy barrier formed by OH* ($\Delta G1 = 3.74$ eV) is the rate-determining step on the bulk phase Co metal site (Co1 in CoBDC-Fc), which is endowed with a weak adsorption energy of OH*. Moreover, the preparation of proton-conducting MOFs with superconductivity is of special significance for fuel cells. For instance, Liu *et al.* prepared a series of UiO-66 [Figure 3E] with different numbers of missing linker defects and systematically studied the influence of the number of defects on the proton electrical conductivity of the samples[84]. Among them, 60-UiO-66-1.8 (60 represents the synthesis temperature and 1.8 the number of defects) prepared with 3-mercaptopropionic acid as a modulator has the best proton conductivity, which is 3×10^{-2} S cm^{-1} at 100 °C and under 98% relative humidity (RH). The acidic sites induced by missing-linker defects further promote the chemisorption of ammonia molecules, resulting in the formation of a richer hydrogen-bond network and hence boosting the proton conductivity to 1.04×10^{-1} S·cm^{-1} at 80 °C, which is one of the highest values among the reported MOF-based proton conductor. Similarly, Basu *et al.* have designed four MOF-808 A, MOF-808 B, MOF-808 C and MOF-808 D with various amounts of missing linker defects and have investigated the role of the defects in modifying the different structural properties of these MOFs and their effect on the proton conductivity[85]. An impressive enhancement in proton conductivity (from 10^{-3} to 10^{-1} S·cm^{-1}) was observed

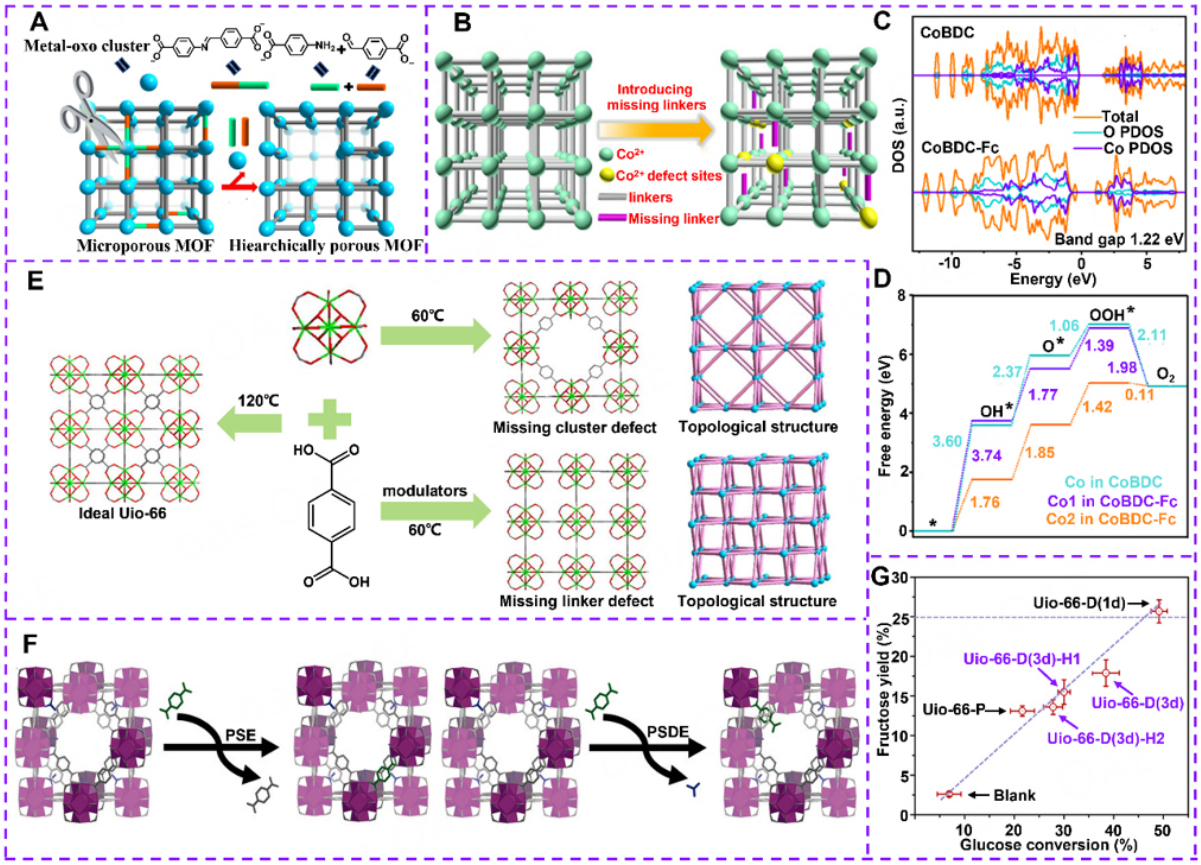

Figure 3. (A) Hierarchical porous MOF developed from the linker labilization. Reproduced with permission[82]. Copyright 2017, Springer Nature. (B) Modulation of the electronic structure of MOF by missing linkers. (C) Calculated DOS of CoBDC and CoBDC-Fc. (D) Free energy diagram for OER on CoBDC and CoBDC-Fc. Reproduced with permission[83]. Copyright 2019, Springer Nature. (E) Structural missing cluster defect or missing linker defect of UiO-66 and the corresponding topological representation. Reproduced with permission[84]. Copyright 2022, American Chemical Society. (F) Post-synthetic ligand exchange and post-synthetic defect exchange. Reproduced with permission[94]. Copyright 2018, Wiley-VCH. (G) Catalytic performances of various UiO-66 samples. Reproduced with permission[73]. Copyright 2019, Springer Nature.

in these four defective MOFs compared to the highly crystalline, low-defect MOF-808 variant. MOF-808 C, having optimized defect density, showed a proton conductivity of 2.6×10^{-1} S·cm^{-1} at 80 °C and 98% relative humidity. The introduction of defects induces super-protonic conductivity by modifying different properties, like porosity, water sorptivity, and acidity.

Missing cluster defects

The framework structure, internal pore size, and pore wall chemical environment of MOFs can be precisely controlled by designing and selecting organic ligands with different lengths and functional groups and inorganic secondary building units (SBUs) with different structural orientations[86]. Among them, some metal-containing inorganic SBUs are deficient in the lattice of MOFs to form cluster defects. The hierarchical porous structure provided by the cluster defect can facilitate the diffusion and adsorption processes of the guest molecules, which leads to enhanced catalytic performance[87-89].

Post-synthetic ligand exchange (PSE) has been demonstrated to be a straightforward and versatile method to introduce functionalities in the crystal structure of well-stabilized MOFs that cannot be obtained via direct synthesis[90-92]. In the case of Zr-based MOFs, during the PSE of defective Zr-MOFs, the exchange may

be done in a competitive manner involving framework linkers and defective compensation groups, with the nature of the defect determining different outcomes, that is, missing linkers[80] or missing clusters[93]. In a special case of missing clusters, the post-synthetic ligand exchange would compete against an alternative of a single carboxyl modulator to coordinate the incoming linker by passing only one of its carboxyl groups, and the process is called post-synthetic defect exchange (PSDE) [Figure 3F][72,94]. Additionally, defect engineering of MOFs opens up a new avenue for tailoring their desired characteristics to meet specific applications[95,96]. Unfortunately, it is still difficult to directly probe the local structure in the crystal and thus determine the defect structure in MOFs, either linker or cluster defects, which has proven challenging. In 2019, Liu *et al.* first investigated defects in MOFs by direct imaging in real space using a low-dose HRTEM technique combined with electron crystallography[73]. These observations provide researchers with insight into the types, distributions, and precise three-dimensional structures of defects in MOF UiO-66. Finally, when these defective materials were used as catalysts for glucose isomerization, the missing clustering defects were found to have stronger catalytic activity than the missing linkers [Figure 3G].

Macroscopic defects

In contrast to linker defects or cluster defects, macroscopic defects of several nanometers to a few micrometers in size are present inside the crystal when linker defects and cluster defects are present adjacent to each other. These defects are obtained intentionally, either by de novo synthesis or post-synthetic modification[74,97-99]. According to recent advances in the preparation of macroscopic defects in MOF structures, the synthesis schemes are mainly divided into two types [Figure 4A]. Monocarboxylic acids (MAs) are commonly used as modulators in the preparation of MOFs. They will coordinate with the metal nodes, and upon removal of the modulators, structural defects and additional pores will be created by the alkyl chains simultaneously[100,101] [Scheme 1]. Additionally, the formation of macroscopic defects can be controlled by varying the length of alkyl chains and the concentration of modulators. The degree of deprotonation of carboxyl groups in organic ligands can be enhanced by organic bases, which in turn scales down the nucleation period of crystal crystallization, resulting in crystals with narrow size distribution. Therefore, macroscopic defects in MOFs can be artificially tailored by introducing organic bases[102] [Scheme 2]. This part mainly discusses the synthesis of macroscopic defects in Uio-66 and MOF-5.

Wang *et al.* proposed a new strategy for the synthesis of MOFs with controlled macroscopic defects using dodecanoic acid (DA) and triethylamine (TEA) as a comodulator[103]. The MOF UiO-66 crystals constructed with linear 1,4-benzenedicarboxylic acid (BDC) ligands and $Zr_6O_4(OH)_4$ clusters as nodes are tunable in the pore size range of 40~270 nm under the combined effect of TEA modulator. In the case of DA only, the synthesized Uio-66 is octahedral or spherical in shape, which has a widespread size distribution. In contrast, discrete nanoparticles of the same shape and relatively homogeneous size can be achieved after the introduction of TEA into the reaction system [Figure 4B-E].

Choi *et al.* demonstrated the heterogeneous distribution of pores in MOF-5 using 4-(dodecyloxy)benzoic acid (DBA)[104]. By controlling the amount of DBA in the reaction system, it was possible to obtain crystals with significantly different distributions of defects: (sponge-like MOF-5) spng-MOF-5 and pomegranate-like MOF-5(pmg-MOF-5) [Figure 4F]. Benefiting from the special structure of pmg-MOF-5, pmg-MOF-5 has strong CO_2 adsorption performance, and under the same conditions, pmg-MOF-5 (2.0 $g \cdot g^{-1}$) adsorbs more CO_2 than MOF-5 (1.5 $g \cdot g^{-1}$). Following a similar approach, Cai *et al.* proposed a facile and universal method of modulator-induced macroscopic defect formation method for the preparation of various hierarchically porous MOFs (HP MOFs) with excellent properties, which led to the artificially controllable preparation of hierarchically porous Uio-66 [Figure 4G] by introducing a series of alkyl carboxylates[105]. Analysis of the SEM and TEM images from Figure 4H and I revealed that worm-like mesopores could be observed in the ideal HP-Uio-66. Surprisingly, the structure of HP-UiO-66 appeared after the defect not

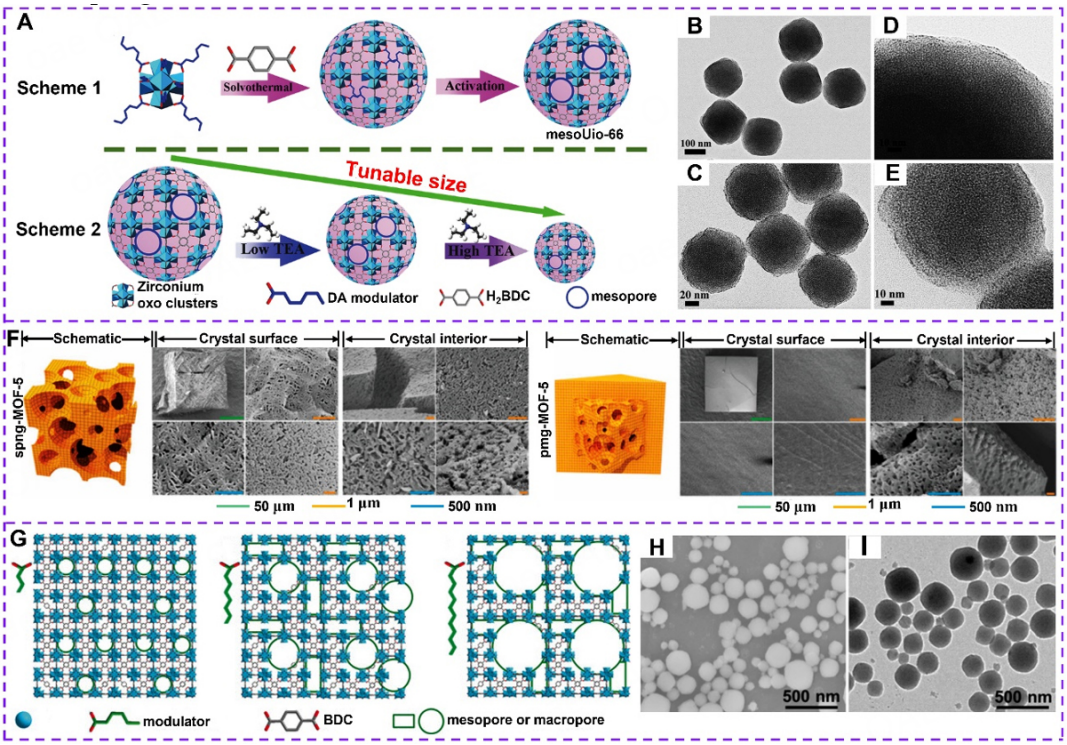

Figure 4. (A) Schematic illustration for the synthesis of large-pore MOFs. (B and C) TEM images of the mesoUiO-66, (D and E) their corresponding magnified images. Reproduced with permission[103]. Copyright 2020, Wiley-VCH. (F) SEM images of Spng-MOF-5 and pmg-MOF-5. Reproduced with permission[104]. Copyright 2011, American Chemical Society. (G) Schematic illustrations of the synthesis of HP-Uio-66, (H) SEM images of HP-UiO-66. (I) TEM images of HP-UiO-66. Reproduced with permission[105]. Copyright 2017, Wiley-VCH.

only did not affect the stability but also improved its catalytic activity. Furthermore, to demonstrate the approach's versatility, various types of HP-MOFs were synthesized by rational design based on stable MIL-53, DUT-5, and MOF-808.

FORMATION OF DEFECTS IN MOFS

According to the previous research reports, there are two main approaches to synthesizing defective MOFs: de novo synthesis approach and post-synthetic modification (PSM) approach. In this Section, we will summarize and discuss the different preparation strategies for the formation of defects in MOFs [Table 2].

De novo synthesis of defects

During the synthesis of MOFs, the formation of defects can be promoted by rational control of the synthesis conditions. The most common methods for forming defects de novo synthesis is mainly modulation approach, mixed linker approach, and fast crystallization approach.

Modulation approach

The modulator approach is the most common strategy used to synthesize defective MOFs[106]. In this method, in addition to organic ligands, a large number of monocarboxylic acids are added during the synthesis to improve the crystallinity of MOFs[107-109]. There are two usual mechanisms for inducing defect formation using modulators: (1) the conjugate acid of the modulator protonates the linker from the node; and (2) the conjugate base of the modulator competes with the linker for coordination to the node[107], resulting in the defect of missing linker[80] and/or missing cluster[110]. The chemistry of the defects formed

Table 2. The relevant publications on synthetic strategies for defective MOFs

Compound	Defective MOFs synthesis strategy	Characterization	Applications	Reference
MIL-100 (Fe)	Etching treatment	PXRD, XPS, TEM, SEM, HRTEM, EDS	-	[101]
Uio-66	solvothermal method	XRD, SEM, TEM, EDS, XPS, FT-IR	Catalysis	[112]
MOF-199	Modulation approach	XRD, FTIR, SEM, N_2 adsorption-desorption, XPS, TG	Sulfide adsorption	[113]
Uio-66	Modulation approach	PXRD, BET, TEM, HRTEM, TGA	Catalysis	[114]
Uio-66	Modulation approach	PXRD, N_2 sorption, dissolution/NMR, TGA-DSC, SEM/EDX, and ATR-IR	-	[95]
Uio-66	Modulation approach	SEM/EDX, PXRD, TGA, BET, FT-IR	Arsenic adsorption/recovery	[117]
Uio-66	Modulation approach	High-resolution neutron power diffraction	Gas adsorption	[80]
HKUST -1	Modulation approach	^{1}H NMR, FT IR, XPS, BET, PXRD, XPS, N_2 sorption isotherms	Gas uptake	[121]
$Ru3(btc)_{2-x}(pydc)_xX_y$	Mixed linker approach	PXRD, FT IR, XPS	Sorption and catalysis	[126]
PCN-133/PCN-134	Mixed linker approach	PXRD, N_2 sorption isotherms	Catalysis	[127]
Uio-66	Mixed linker approach	PXRD, TGA, N_2 physisorption, NMR	-	[128]
Uio-66	Mixed linker approach	PXRD, TGA, ^{1}H NMR, BET, SEM	Catalysis	[130]
ZIF-8	Fast crystallization approach	PXRD, SEM, FT IR, N_2 adsorption	Catalysis	[131]
Uio-66	Fast crystallization approach	PXRD, SEM, FT IR, TGA, BET, XPS, N_2 adsorption-desorption	Catalysis	[132]
MOF-5	Thermal treatment	PXRD, FT-IR, XPS, TGA	Gas uptake or separation	[135]
MIL-101(Cr)	Thermal treatment	PXRD, FT-IR, TGA, TEM, XPS	Catalysis	[136]
ZIF-8	Mechanical treatment	PXRD, SEM, FT-IR	Drug delivery	[137]
HKUST-1	Mechanical treatment	PXRD, N_2 sorption isotherms, TGA, XPS, 1H NMR, GC	CO_2 sorption and catalytic	[138]
HKUST-1	Etching treatment	PXRD, TGA, SEM, NMR, BET	Catalysis	[141]
HKUST-1	Etching treatment	PXRD, N_2 sorption isotherms, SEM, BET	-	[142]
Al-bpydc	Etching treatment	PXRD, SEM, TEM, XPS, NMR, N_2 adsorption-desorption isotherms	Catalysis	[143]
Co-MOF	Etching treatment	FESEM, XRD, EDX	Catalysis	[144]
Pt@UiO-66-NH_2, Pt@UiO-66, Pt@ZIF-8, and Au@ZIF-8	Thermal treatment	PXRD, FT-IR, TGA, HRTEM, N_2 adsorption-desorption isotherms, EXAFS	Catalysis	[145]
Uio-66, MIL-101	Thermal treatment	PXRD, XPS, SEM, N_2 adsorption-desorption isotherms	Gas adsorption	[146]
Uio-66/MIL-140B/MIL-140C	Mechanical treatment	PXRD, ^{13}C NMR, IR	-	[147]
MIL-53	Mechanical treatment	PXRD, XRD, BET, FT-IR	C_2H_2 storage	[148]

during the synthesis of MOFs is closely related to the type and number of modulators used. Up to now, several classical monocarboxylate modulators, such as formic acid (FA)[111], acetic acid (AA)[89,112,113], trifluoroacetic acid (TFA)[114], dichloroacetic acid (DCA)[115], difluoro acetic acid (DFA)[95], and L-phenylalanine (L-Phe)[116], have been frequently introduced into MOFs to induce defect formation.

In 2016, Shearer *et al.* proposed a close correlation between the acidity (pKa) and/or concentration of modulators and the defect concentration in the framework of MOFs[95]. They have systematically explored the effect of various modulators (AA, DFA, and FA) on Uio-66 defect concentration. They found that the defect concentration was positively correlated with the modulator acidity/pKa [Figure 5A]. The pKa or concentration of modulators can be reasonably controlled to regulate the density of defects in MOFs. Furthermore, all the modulators selected in this study were completely miscible with the solvent, thus neglecting the possibility that solubility may affect the synthesis in the defective MOFs. Therefore, it is

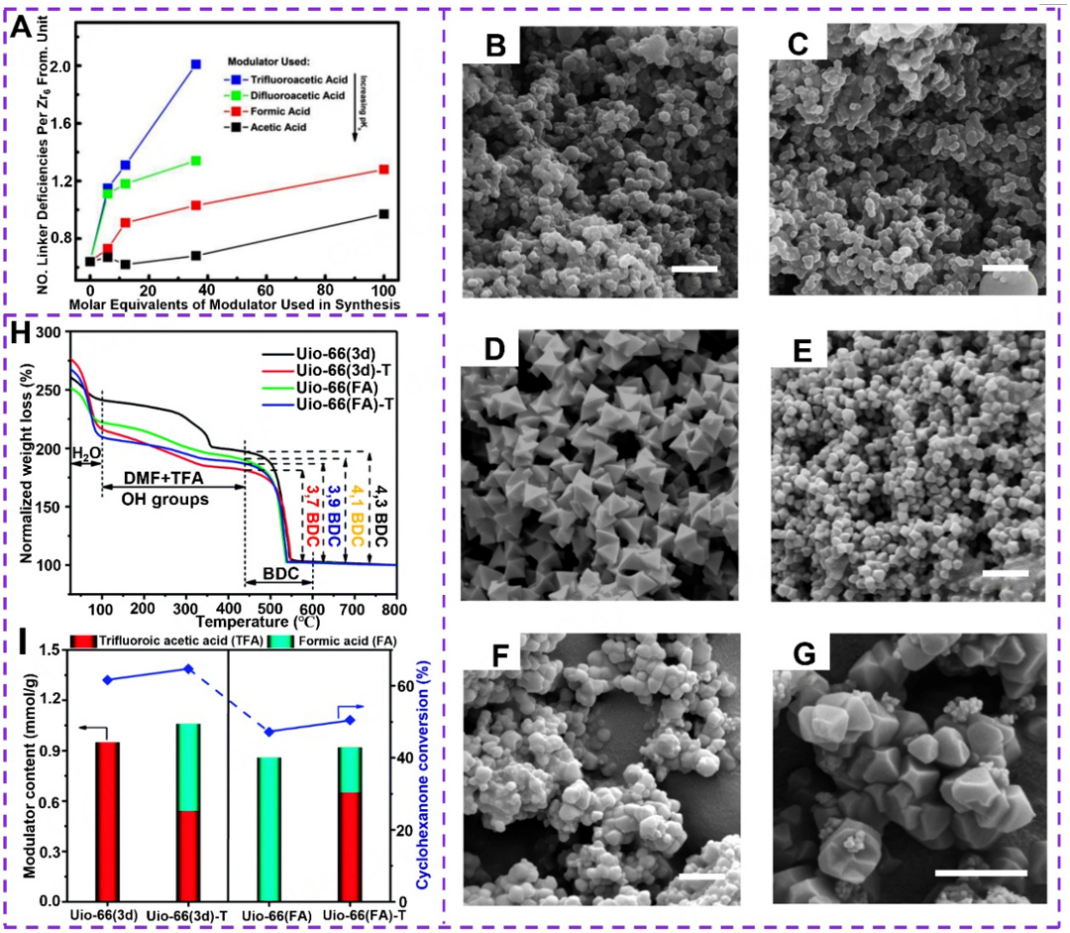

Figure 5. (A) The number of defective linkers per Zr_6 formula unit against modulator molar equivalents in UiO-66. Reproduced with permission[95]. Copyright 2016, American Chemical Society. (B) SEM images of the studied MOF nanoparticles UiO-66, (C) UiO-66-12AA, (D) UiO-66-36AA, (E) UiO-66-100AA, (F) UiO-66-12TFA, and (G) UiO-66-36TFA. Reproduced with permission[117]. Copyright 2020, American Chemical Society. (H) TGA curves, and (I) catalytic performance over these UiO-66 samples. Reproduced with permission[114]. Copyright 2020, The Royal Society of Chemistry.

essential to consider the effect of modulator solubility or steric effects in the synthesis process in defective MOFs, besides the influence of the acidity and concentration of the modulator on the formation of defects in the framework of MOFs. Recently, Assaad *et al.* found that the distribution density of defects could be effectively regulated and controlled by changing the type and amount of the modulator, such as using different ratios of acetic acid and trifluoroacetic acid as the modulator of Uio-66 and HRSEM researched the morphology of Uio-66, and the SEM images are shown in Figure 5B-G[117]. Among them, trifluoroacetic acid causes a larger volume of defects than acetic acid, and the higher the proportion of the modulator, the higher the distribution density of defects formed. In addition, Wu *et al.* proposed that the concentration of defective missing linkers could be effectively regulated by reasonably varying the modulator concentration and synthesis time, thus increasing the porosity and further improving the gas adsorption performance of the defective MOFs[80].

MOF structures have promising applications in catalysis due to their high density of metal nodes. Unfortunately, the metal nodes in MOF structures are completely occupied by organic ligands, resulting in catalytic performance rarely superior to that of microporous solid catalysts (such as zeolites)[118,119]. Therefore, tuning the active sites in the structure of MOFs to improve their catalytic activity remains a large

challenge. In 2020, Wang *et al*. reported the preparation of defective MOF Uio-66 with trifluoroacetic acid (TFA) as a modulator and systematically investigated it as a catalyst for the liquid reaction of cyclohexanone to cyclohexanol *via* hydrogen transfer[114]. Not all structural defects are catalytic for cyclohexanone. Only the open metal sites generated by the modulating agent are effective for the catalytic conversion of cyclohexanone [Figure 5H and I]. According to the findings, under identical reaction circumstances, missing linker defects and missing cluster defects created an increase in the quantity of functional open metal sites and enhanced their catalytic activity. In 2019, Kang *et al*. first proposed a new strategy of templated electrosynthesis of vacancy MOFs using ionic liquids as electrolytes and templates[120]. The mesoporous Cu(II)-MOF MFM-100 was successfully prepared by the rapid electrosynthesis method, and the presence of defects in Cu(II)-MOF MFM-100 was confirmed by advanced characterization methods. Additionally, in recent years, many researchers have synthesized a series of hierarchically porous MOFs by controlling the reaction conditions of the modulation approach, such as the introduction of mesopores in microporous MOFs, thus making the application of MOFs more extensive[121-123]. The modulation approach is widely used by researchers as a more mature method.

Mixed linker approach

The mixed linker approach is a common strategy for introducing defects in MOFs. As the name implies, it involves directly adding two or more structurally similar organic linkers as precursors to the reaction. According to the type of mixed linkers, they can be mainly divided into isostructural mixed linker (IML) and heterostructural mixed linker (HML)[124]. Different linkers can be mixed to form defective MOFs with different sizes, shapes, and porosities[74,125]. The location of defects in MOFs synthesized by mixed organic linkers depends on the relative rates of coordination bond formation and exchange. If the framework growth rate is faster than the exchange rate, the defects will be contained in the framework, and if the exchange rate is faster than the framework growth rate, the defects will reside on the crystal surface.

In 2014, Kozachuk *et al*. reported the synthesis of a series of single-phase defect variants $Ru_3(btc)_{2-x}(pydc)_xX_y$] (D1-D4) by using mixed linkers of 1,3,5-tricarboxylate (H_3btc) and pyridine-3,5-dicarboxylic acid (H_2pydc) [Figure 6A][126]. The structure and charge distribution of linkers btc^{3-} and $pydc^{2-}$ are very similar, but $pydc^{2-}$ has one less carboxylate ligator site compared to btc^{3-}. And $pydc^{2-}$ acts as a second defective linker, leading to the formation of the defect in Ru-MOF. In addition, the incorporation of $pydc^{2-}$ induced the reduction of some Ru metal sites. In 2016, Yuan *et al*. proposed a strategy using the thermodynamically guided synthesis of mixed linker Zr-MOFs with pillared-layer structure, namely PCN-133 and PCN-134 [Figure 6B][127]. Among them, PCN-134 not only shows high porosity and excellent chemical stability, but also maintains the integrity of its framework, while tolerating the absence of some auxiliary linkers, so that the defect density can be controlled by reasonably adjusting the ratio of auxiliary linkers to further improve the performance of PCN-134. The thermal stability of the modulator also contributes critically to the formation of defects. In 2017, Bueken *et al*. exploited the difference in decomposition temperatures of BDC (terephthalic acid) and CDC (*trans*-1,4-cyclohexanedicarboxylate) linkers to successfully introduce missing linker defects in the mixed linker UiO-66 [Figure 6C], thus also providing researchers with a comprehensive insight into the relationship between defect structure and properties of UiO-66 MOFs[128].

Moreover, as the research on MOFs is intensified, they are oriented to a wider range of applications. At present, many MOFs have been functionalized by introducing organic ligands with different functional groups. In 2010, Deng *et al*. conducted a series of systematic research[129]. Based on MOF-5, they first introduced functional groups $-NH_2$, -Br, $-(Cl)_2$, $-NO_2$, $-(CH_3)_2$, $-C_4H_4$, $-(OC_3H_5)_2$ and $-(OC_7H_7)_2$ into BDC structure, and then selected two or more of these ligands to synthesize 18 types of MTV-MOF-5

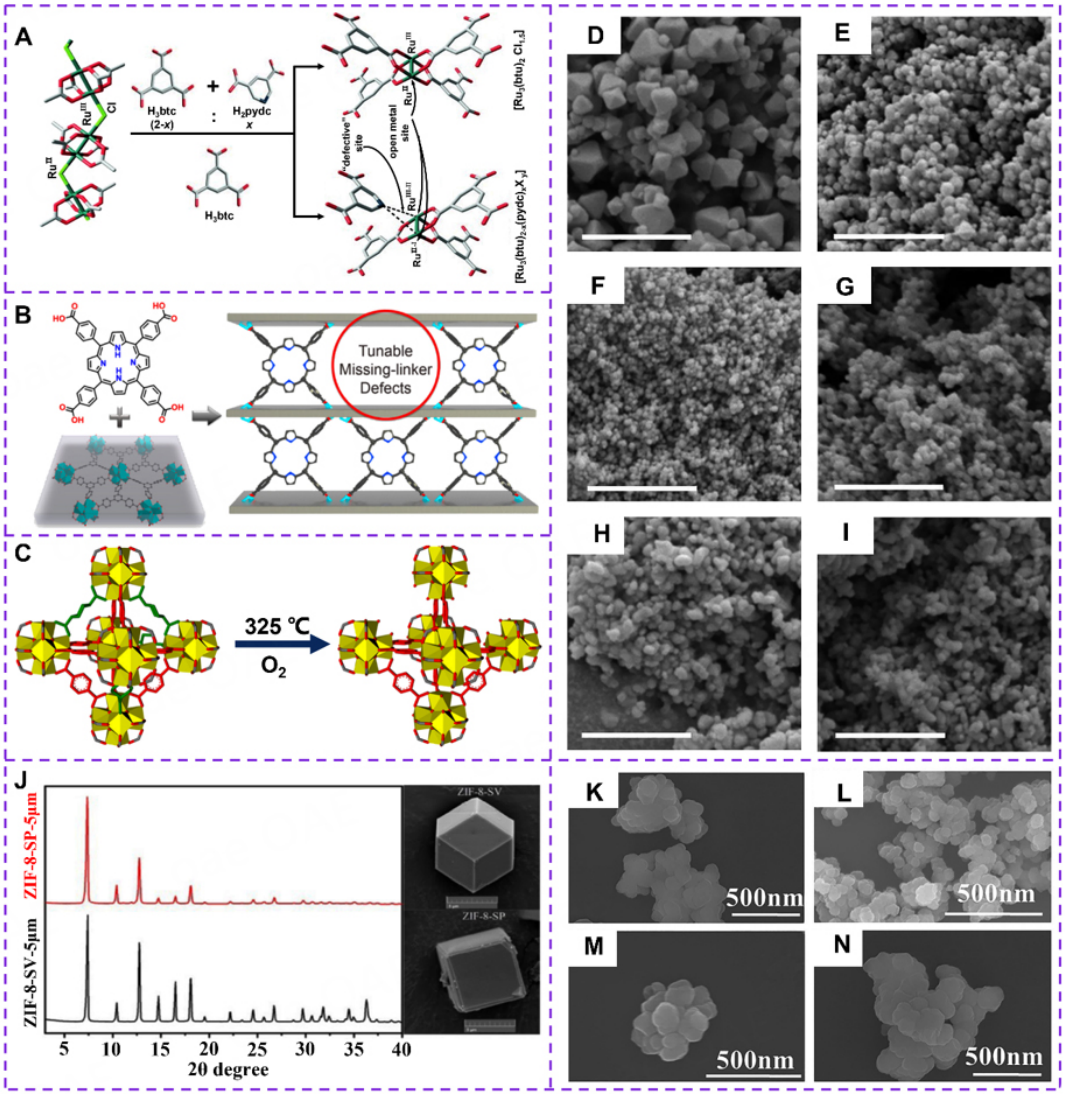

Figure 6. (A) Mixed linker approach in Ru-HKUST-1 leads to modified node defects. Reproduced with permission[126]. Copyright 2014, Wiley-VCH. (B) PCN-134 formed by 6-connected Zr 6 cluster, BTB, and TCPP. Reproduced with permission[127]. Copyright 2016, American Chemical Society. (C) Schematic illustration of defect formation by thermal decomposition of labile linker. Reproduced with permission[128]. Copyright 2017, American Chemical Society. SEM images of MTV Uio-66, (D) UiO-66(3A:1B), (E) UiO-66(1A:1B), (F) UiO-66(1A:3B), (G) UiO-66(3A:1C), (H) UiO-66(1A:1C) and (I) UiO-66(1A:3C). Reproduced with permission[130]. Copyright 2021, Elsevier. (J) The XRD patterns of ZIF-8-SV-5 μm and ZIF-8-SP-5 μm (insert SEM images). Reproduced with permission[131]. Copyright 2017, Elsevier. SEM images of UIO-66 with different synthesized conditions, (K) Zr-H-2 h, (L) Zr-H-10 h, (M) Zr-H-120 °C, (N) Zr H-140 °C. Reproduced with permission[132]. Copyright 2021, Wiley.

(Multivariate MOFs), which are similar structure to MOF-5 and have various functionalization. Recently, Jrad *et al.* proposed the combination strategy of multivariate approach with modulated synthesis to develop two highly defective and functionalized MTV-UiO-66 series, namely MTV-UiO-66(COOH)$_2$ and MTV-UiO-66(OH)$_2$, and the SEM images are shown in Figure 6D-I[130]. Furthermore, the comparative analysis of 33 different UiO-66 catalysts for the conversion of butyl butyrate showed that the density of active sites, as well as the number of defects or the number of functional groups on the linker, had a greater influence on the conversion of butyl butyrate relative to the surface area and catalyst loading level. These findings also provide a theoretical basis for expanding the application of Uio-66 in biofuel catalysts.

Fast crystallization approach

In addition, the fast crystallization approach is another effective strategy for creating defects in the MOF structure. The fast crystallization approach is mainly assisted by microwave-assisted synthesis and the addition of high concentrations of precursors to promote the fast crystallization of MOF crystals resulting in defects. Depending on the effect of modulators on MOFs in terms of reaction kinetics and crystallinity, the fast crystallization process leads to the formation of defects, such as ligand or metal center defects[76]. In 2017, Chaemchuen *et al.* synthesized three different types of defective ZIF-8 [Figure 6J], MOF-5 and Zn-DABCO using a fast crystallization strategy and compared their catalytic properties on this basis[131]. The defects formed in MOFs due to different crystal growth rates were found to affect the structure, morphology and other properties of the materials, such as particle shape and specific catalytic properties. Recently, Chu *et al.* used concentrated hydrochloric acid as a modulator to design and synthesize a series of defective Uio-66 by a rapid crystallization method [Figure 6K-N][132]. The prepared defective Uio-66 not only has the advantages of low preparation temperature, short preparation time and large-scale preparation but also removal of DBT from ODS exhibits excellent catalytic performance. More importantly, the fast crystallization approach provides a new strategy for introducing defects in the structure of MOFs, further expanding the application prospects of MOFs materials.

Defects created by postsynthetic treatment

In addition to defect modulation by de novo synthesis, postsynthetic treatment is another significant way to form defects in MOFs, such as etching treatment[133,134], pyrolysis treatment[135,136], and mechanical treatment[137,138].

Etching treatment

Postsynthetic treatment refers to the MOFs activation and purification while maintaining the structural integrity of materials. Etching is an ancient fabrication method and one of the simplest and most efficient to generate defects among MOFs during the post-synthesis process[139]. Therefore, replacing the linker in the MOF framework with an acid/base group may create defects in the post-synthetic parent MOF[133,140]. For example, in 2017, Koo *et al.* reported a new strategy for introducing mesopores into water-stabilized microporous MIL-100(Fe) using a selective acid etching process [Figure 7A][101]. Due to the selective nature of the etching process, this method preserves the inherent crystallinity and external morphology of MIL-100(Fe) on the basis of allowing fine-tuning of the porosity [Figure 7B and C]. In addition, this strategy was also shown to be applicable to the synthesis of mesopores introduced in other water-stabilized microporous MOFs. In addition to acid etching, gas etching has also been applied to create defects in the framework of MOFs. On the contrary, in 2019, Doan *et al.*, inspired by the fact that phosphoric acid can tune the porosity of MIL-100(Fe) by selective acid etching, successfully prepared defective hierarchical porous MOFs framework by phosphoric acid as an etching agent in water unstable HKUST-1 MOF[141]. At the same time, it was also demonstrated that the extent of etching on MOFs was affected by the combined effect of pH and etching time. Recently, Albolkany *et al.* proposed an ammonia gas phase etching method to format mesopores within carboxylate-based microporous MOFs (HKUST-1, [Cu_3BTC_2], BTC = 1,3,5-benzenetricarboxylic acid) and thus produce hierarchically porous MOFs [Figure 7D][142]. Ammonia as gas phase etching agent is first uniformly adsorbed into the microporous MOFs, ensuring uniform etching within the MOFs crystal. The mesopores were prepared under heated conditions by cutting the carboxyl-metal coordination bonds using the strong coordination between ammonia and metals. In the HKUST-1 model, the size of the mesopores is controlled by the etching temperature and the volume of the mesopores can be modulated by changing the pressure of the etchant ammonia [Figure 7E and F]. This strategy can precisely control the mesopore size and volume without affecting the crystal morphology.

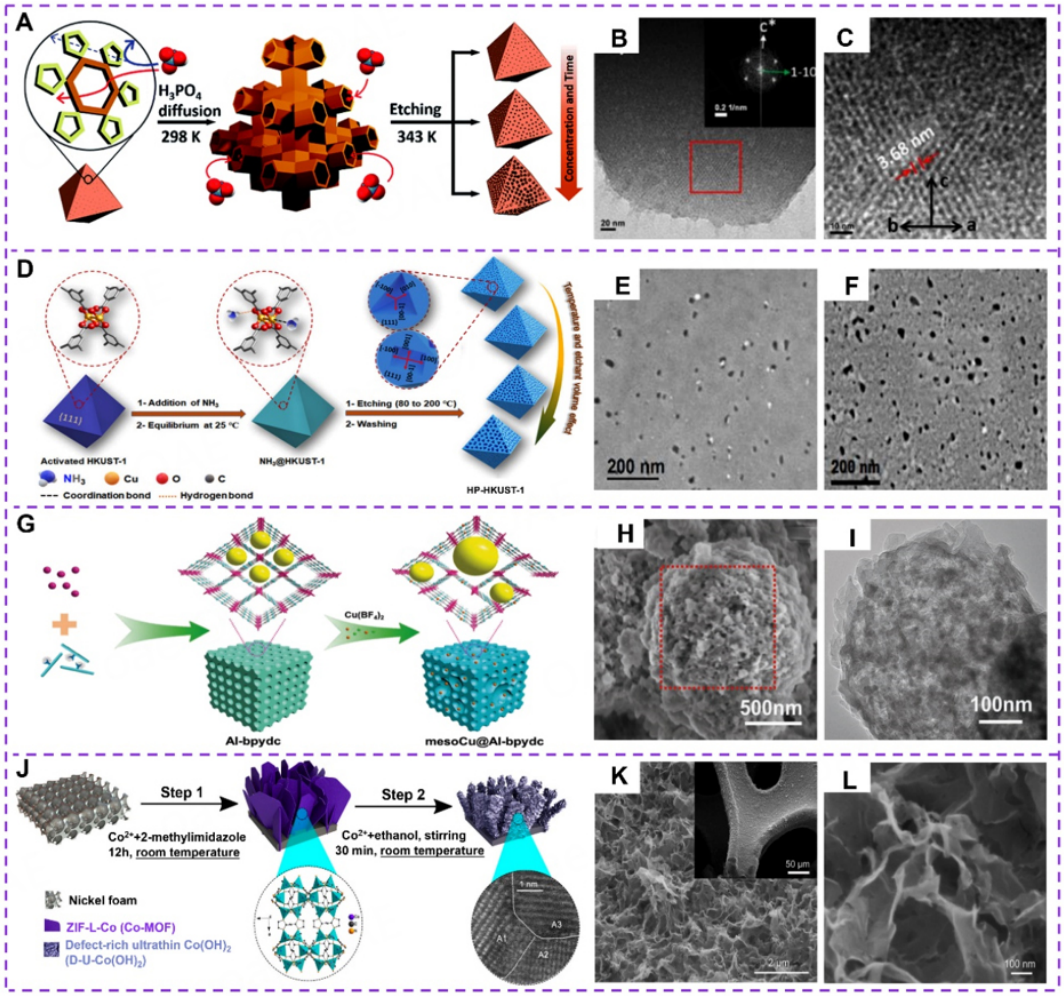

Figure 7. (A) Illustration of the etching process for MIL-100(Fe), (B and C) TEM images of MIL-100(Fe)-40. Reproduced with permission[101]. Copyright 2017, The Royal Society of Chemistry. (D) Schematic illustration of the formation of hierarchically porous MOF by ammonia etching of HKUST-1, (E) SEM images of HP-HKUST-1 prepared using 20 mL NH_3 at 160 °C, (F) SEM images of HP-HKUST-1 prepared using 20 mL NH_3 at 200 °C. Reproduced with permission[142]. Copyright 2021, Wiley-VCH. (G) Schematic illustration of the synthesis of mesoCu@Al-bpydc. (H) SEM images of mesoCu@Al-bpydc, (I) TEM images of mesoCu@Al-bpydc. Reproduced with permission[143]. Copyright 2019, Wiley. (J) Schematic illustration of the synthesis pathway of Co-MOF and the generation of polycrystalline 2D materials at room temperature. (K and L) SEM images of Co-MOF nanoarray-derived. Reproduced with permission[144]. Copyright 2018, American Chemical Society.

In 2019, Chang *et al.* proposed a facile and original *in situ* defect formation strategy to construct hierarchical MOFs using tetrafluoroborate [$M(BF_4)_x$] as both the functional site and etching agent[143]. Firstly, microporous MOF Al-bpydc (bpydc = 2,2′-bipyridine-5,5′-dicarboxylic acid) and $Cu(BF_4)_2$ were selected as the parent MOFs and tetrafluoroborate, respectively, and then $Cu(BF_4)_2$ was doped into Al-bpydc by wet impregnation method. Thus mesoCu@Al-bpydc was constructed [Figure 7G-I]. This strategy not only maintains the structural stability of MOFs, but also rationally designs and controls the chemical environment of hierarchically porous MOFs. Furthermore, the nanoscale engineering of crystal boundary defects can significantly improve the catalytic activity of nanoelectrocatalysts in reactions such as OER and CO_2 reduction. Therefore, theoretically, the introduction of nanoscale crystal boundary defects within 2D materials can further improve the electrocatalytic performance of 2D materials. In 2018, Zhang *et al.* first synthesized Co-MOF nanosheet arrays as precursors at room temperature, and then obtained three-dimensional network structures of nanoscale polycrystalline two-dimensional nanosheets by etching/

reconfiguration of MOF in an ethanol solution system at room temperature [Figure 7J-L][144]. The material exhibited excellent OER activity and stability under alkaline conditions.

Pyrolysis treatment

Post-synthetic thermal treatment is a rapidly modifying method for changing the structure and properties of metals and polymers, and an efficient alternative method for creating defects in MOFs. The linker defects or cluster defects may be created through the control of the temperature and heating time of the decomposition of specific organic groups during the calcination process. In 2014, Gadipelli *et al.* proposed a facile and versatile method to promote the decomposition of carboxylate BDC (BDC = benzene dicarboxylate, -OOC-C_6H_4-COO-) by thermal annealing of the MOF post-synthesis below the framework decomposition temperature, resulting in the formation of defects in MOF-5 [Figure 8A][135]. The results showed that the annealed MOF-5 exhibited excellent CO_2 adsorption capacity compared to the untreated MOF-5 with a maximum uptake of 2 mmol·g^{-1} at the same conditions of 25 °C and 1 bar. Nanoparticle@MOFs composites have attracted much attention from researchers for their excellent selective catalytic performance. However, there is an urgent need to investigate a simple method to solve the balance between catalytic efficiency and selectivity. For instance, Meng *et al.* proposed to successfully prepare Pt@UiO-66-NH_2, Pt@UiO-66, Pt@ZIF-8, and Au@ZIF-8 with hierarchical porosity by taking advantage of the thermal instability of the inherent defects of the encapsulated nanoparticles and selecting a suitable temperature annealing [Figure 8B][145]. where the position and dispersion of mesopores can be located and controlled, respectively. Unexpectedly, the resulting Pt@UiO-66-NH_2 exhibited not only enhanced catalytic efficiency but also improved catalytic rate and selectivity. In addition, this approach can also be extended to be applied to other MOFs and their derivatives for the production of hierarchical porous structures due to the prevalence of structural defects in MOFs. Recently, Jia *et al.* have proposed an air-heat treatment strategy to investigate with the assistance of high enthalpy pressurized air to remove residual molecules and incompletely coordinated linkers from MOFs in order to maximize the porosity of the obtained MOFs[146]. [Figure 8C] The obtained MOFs with hierarchical micro/mesoporous structures exhibited excellent adsorption capacity and selectivity, such as CuBTC-A (BTC = 1,3,5-benzenetricarboxylic acid) obtained after thermal treatment of CuBTC improved CO_2 uptake and CO_2/N_2 selectivity by 22% and 86%, respectively.

Moreover, post-synthesis thermal treatments are becoming increasingly popular among researchers as a common approach to optimize the structure and improve the performance of MOFs, and numerous MOF-derived materials were designed and synthesized. However, the wide selection of extreme thermo-treatment conditions (typically above 500 °C) not only does not improve the performance of MOFs, but also leads to the degradation of intrinsic properties. In 2020, Pan *et al.* calcined MIL-101(Cr) in the range of 200-280 °C and investigated the effect of the thermal treatment at different temperatures on MOFs and revealed that the thermal treatment could introduce unsaturated CrO_x clusters and generate partial deligandation [Figure 8D-F][136]. Calcinating MIL-101(Cr) at 280 °C created defects as active catalytic sites that improved the oxidation activity of styrene, which was ten folds more active than that of the original MIL-101.

Mechanical treatment

Mechanical treatment is a physical means to break the coordination bonds in the structure of MOFs, resulting in structural defects in the framework. In 2016, Bennett *et al.* ball-milled MOFs to break the metal-ligand bonds in parts of the framework of MOFs such as UiO-66, MIL-140B and MIL-140C[147]. DFT calculations confirm the existence of defects in the MIL-140B framework. At the same time, the mechanical treatment strategy is also applicable to ZIF-8 and MIL-53[137,148]. Recently, Steenhaut *et al.* treated HKUST-1 with ball milling and found that the number of defects was related to the duration of milling, and CO_2

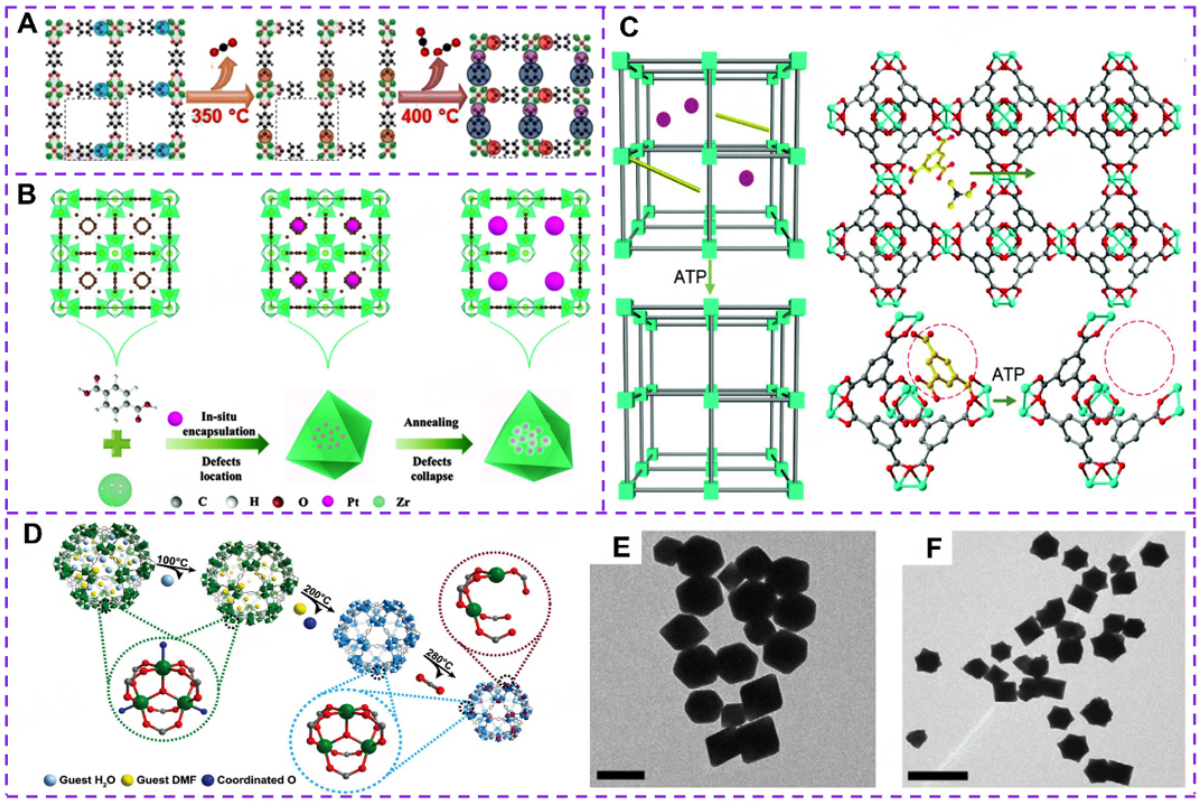

Figure 8. (A) Schematic illustration of framework formation defect due to MOF-5 annealing. Reproduced with permission[135]. Copyright 2014, American Chemical Society. (B) Schematic illustration of the synthesis of hierarchically porous Pt@MOFs using inherent defects. Reproduced with permission[145]. Copyright 2018, Wiley-VCH. (C) Schematic of air-thermal processing strategy. Reproduced with permission[146]. Copyright 2020, The Royal Society of Chemistry. (D) Schematic illustration for the structural evolution of MIL-101 under thermal treatment, (E) TEM image of Uio-66, (F) TEM image of Uio-67. Reproduced with permission[136]. Copyright 2020, Wiley-VCH.

adsorption experiments showed that the adsorption capacity of HKUST-1 was mainly dependent on the type and number of defects in MOFs rather than their surface area[138]. Although mechanical treatment is much simpler compared with other post-synthetic modification processes and can control the number of defects formed, it is still difficult to control the type of defects introduced, so mechanical treatment can be combined with other post-synthetic modification methods to jointly regulate and thus synthesize MOFs with excellent properties.

CATALYTIC APPLICATIONS OF DEFECTS IN MOFS

Over the past few years, MOFs and their derivatives have attracted much attention in the field of heterogeneous catalysis and energy storage due to their diverse structures and high porosity[149-151]. On the one hand, defective MOFs maintain the original structural features without destroying the structure of the parent MOFs[152]. Therefore, the porous nature and high specific surface area of MOFs, as well as the introduction of cluster defects or linkers defects, can improve the utilization of active sites in catalytic reactions[153,154]. On the other hand, the thermal treatment of MOF derivatives will create defects in the structure as active catalytic sites, thus improving the catalytic performance[155].

Catalysis

The porous nature, high specific surface area and available Lewis acidic active sites of MOFs and MOF derivatives imply their wide application in heterogeneous catalysis. It is shown that the introduction of

defects in MOFs and MOF derivatives facilitates the modulation of the electronic structure of the catalyst as well as the increase of the catalyst's active sites[156]. Furthermore, MOFs and MOF derivatives with abundant defects are more likely to adsorb and activate reactants, which is beneficial to further improve the catalytic performance[157,158]. Consequently, it is very attractive to improve the performance of catalysts by modulating the defects of MOFs and MOF derivatives[159].

Photocatalysis

Defects in MOFs and MOF derivatives can improve the photocatalytic ability of the materials mainly through two aspects: inhibition of electron-hole complexation and optimization of the energy band structure[160,161]. Additionally, two parts of the energy barrier are involved in the photocatalytic process: the absorption of light by the ligand (E_{abs}) and the energy required to transfer photogenerated electrons to the unoccupied d orbitals of the metal (E_{LMCT}). The absence of ligands or clusters exposes varying degrees of metal sites, changing the reaction energy barrier and affecting photocatalytic performance[162].

The generation of structural defects is often accompanied by a series of changes such as chemical bond breaks and reorganization, lattice distortion, and electron localization, which in turn have a very important impact on the physicochemical properties of the material[163]. As the investigation progressed, researchers discovered that structural defects can in many cases enhance the properties of materials and even give them novel functions. Therefore, how to optimize the performance by creating structural defects in a rational way has received much attention from researchers in recent years. In 2019, Ma *et al.* used a zirconium-based MOF with excellent stability and easily tunable structure, UiO-66-NH_2, as a model for their study[89]. The degree of linker defects in the structure was tuned by varying the amount of modulator acetic acid during the synthesis process to obtain UiO-66-NH_2-X with a progressively increasing degree of defects, and Pt@UiO-66-NH_2-X was further obtained by introducing co-catalyst Pt nanoparticles into the MOFs pores [Figure 9A]. More interestingly, when the introduction of the modulator in the synthesis reaches a certain level, further increase in its content leads to a further increase in the degree of defects and the photocatalytic hydrogen production activity does not continue to increase but appears to drop. The structural defects and photocatalytic performance showed a very interesting volcano-type variation trend overall [Figure 9B and C]. At the same time, the MOFs have good photocatalytic cycling stability. The results suggest that the presence of MOF structural defects can modulate the photocatalytic performance of the material, and that creating the right number of structural defects is essential for optimizing the performance. However, the investigation of how the defect type and the degree of ligand vacancies in UiO-66 tune the photocatalytic performance have not been found. Wang *et al.* prepared a series of UiO-66-NH_2 with different defect types and various vacancies degree by altering dicarboxylate ligands [Figure 9D], and used them to study their photocatalytic CO_2 reduction performance[162]. The experimental results showed that the ligand-defective UiO-66-NH_2-ML-100 exhibited optimal photocatalytic activity with a maximum photocatalytic CO yield of 21.3 $\mu mol \cdot g^{-1} \cdot h^{-1}$, which was 2.2 times higher than that of the cluster defective UiO-66-NH_2-MC-150 [Figure 9E and F]. DFT calculations show that the introduction of ligand defects produces defective states dominated by ligand unsaturated Zr clusters, decreasing the E_{LMCT}, and electrons are easily excited from the ligands to the unoccupied d orbitals of the metal Zr atoms, improving the photocatalytic efficiency. The cluster defective MOFs, on the other hand, reduce the light absorption capacity (increases E_{abs}) and weaken the photocatalytic activity due to the lack of metal clusters and surrounding connected ligands.

Moreover, introducing defects into MOFs can promote their electron-hole separation and thus improve the photocatalytic activity of the materials. Jiang *et al.* selected HCl as the modulator to synthesize the defective MIL-53 (TEM images are shown in Figure 9G-K) with increased specific surface area and easier electron-

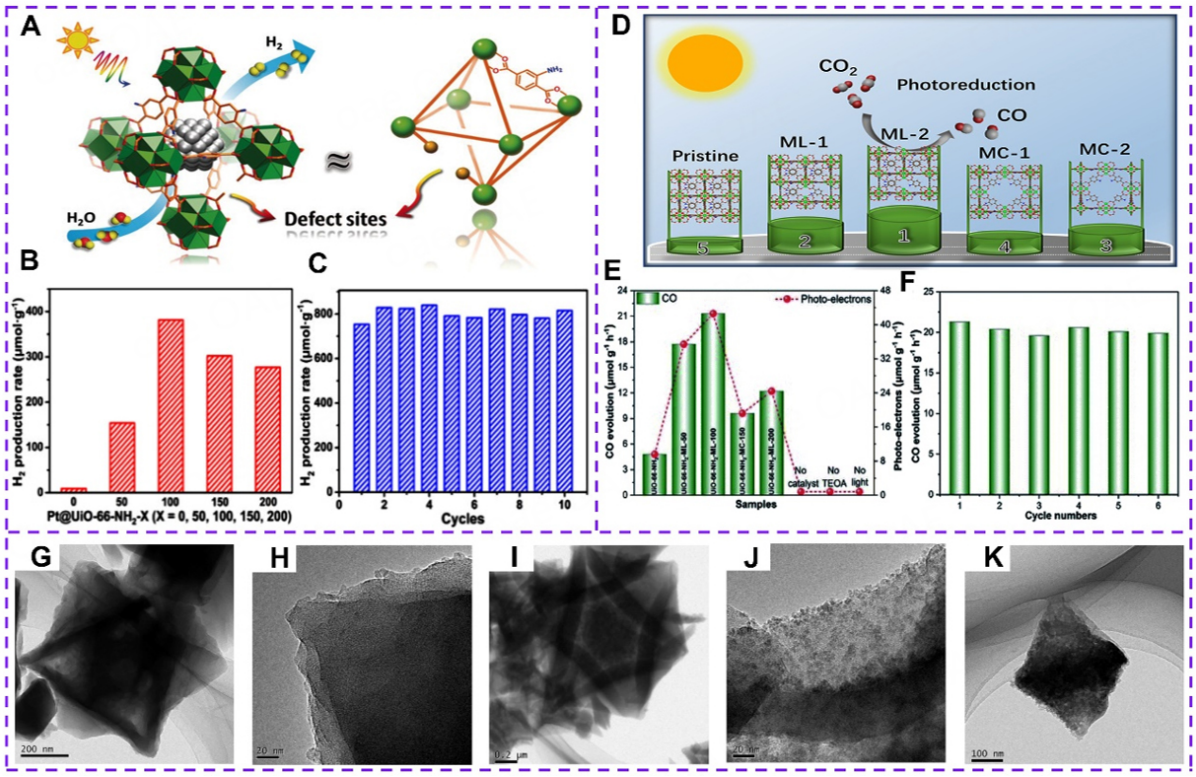

Figure 9. (A) Photocatalytic hydrogen production over Pt@UiO-66-NH_2-X with structural defects, (B) Trends in volcanic type activity of Pt@UiO-66-NH_2-X with different degrees of defects, (C) 10-round activity cycle study of Pt@UiO-66-NH_2-100. Reproduced with permission[89]. Copyright 2019, Wiley-VCH. (D) Application of UiO-66 with different ligand vacancy degrees and defect types for photocatalytic reduction of CO_2, (E) Photoreduction of CO_2 to CO, (F) recycling performance. Reproduced with permission[162]. Copyright 2022, The Royal Society of Chemistry. (G and H) TEM images of MIL-53, (I and J) TEM images of D-1, (K) TEM images of D-2. Reproduced with permission[164]. Copyright 2019, Elsevier.

hole separation[164]. More unexpectedly, when the tetracycline concentration was 10 mg·L^{-1}, the photocatalytic degradation efficiency of defective MIL-53 for tetracycline could reach more than 95%, and the photocatalytic activity was 1.5 times higher than that of the intact MIL-53. However, the design of catalysts and reaction interfaces for directly converting permanent gases (such as CO_2, O_2, and N_2) into liquid fuels is still extremely challenging. Recently, Hao *et al.* proposed that gas-permeable MOF membranes can facilitate the diffusion, activation, and reduction of gas molecules (e.g., CO_2, O_2) through modification of the electronic structure and catalytic properties of metal single atoms[165]. Under visible light irradiation conditions, the MOF NH_2-UiO-66 containing specific defects with Ir single atom as the active center reduces CO_2 to HCOOH at the three-phase reaction interface at 420 nm with an apparent quantum efficiency of 2.51%.

Electrocatalysis

MOFs and their derivatives are regarded as one of the most promising electrocatalytic materials because of their various active sites and easy modification[7]. However, the low electrocatalytic activity and poor electrochemical performance of most MOFs hinder the electrochemical reaction process. Therefore, enhancing active sites in MOFs and their derivatives is important for designing and developing novel and high-efficiency electrocatalysts[166,167]. In recent years, researchers have found that defective engineering can effectively increase the active sites and accelerate the catalytic process, such as OER, HER, ORR, and CO_2 RR.

OER: The OER has a vital role to play in many energy conversion technologies. However, the kinetic process of OER is slow, the efficiency of the reaction remains very low even with the help of noble metal catalysts, and the high cost and scarcity of noble metal catalysts hinder its large-scale application, and it is challenging to develop non-precious metal OER electrocatalysts with high catalytic activity and stability[168,169].

The MOF materials with isolated active sites and large specific surface areas are candidates for high-efficiency catalysts[170,171]. In 2018, Xu *et al.* cleverly prepared hollow structured CoS nanocages using metal organic frameworks (MOFs) as self-sacrificing templates, and then grew CeO_x nanoparticles *in situ* on the CoS surface to achieve precise tuning of the Co^{2+}/Co^{3+} ratio and the generation of active defect sites [Figure 10A], thus significantly facilitating the water oxidation process[172]. Meanwhile, the protective layer of CeO_x formed on the hollow structured CoS surface can effectively prevent the oxidation of CoS and the corrosion loss of the active component elements; thus, the catalyst also exhibits excellent stability [Figure 10B-G]. The method also provides a novel idea to explore for the synthesis of efficient and stable non-noble gold-based electrocatalyst materials. Up to now, the methods available to improve the performance of MOFs-based electrocatalysts are mainly divided into two types: direct synthesis and post-treatment. Among them, post-treatment mainly introduces defects in the structure of MOFs in a targeted manner, which leads to the appearance of electron localization, lattice distortion and chemical bond breakage, thus increasing the active sites and improving the local properties. Therefore, Zou *et al.* selected CoCu-MOF as the target of their study[173]. Firstly, the CoCu-MOF was thermally treated to eliminate some of the functional groups to form defects while retaining the original framework structure of CoCu-MOF. Secondly, the defective CoCu-MOF was phosphorylated to form a highly active CoP/MOF, and the electrocatalyst shows a low overpotential of 295 mV at 10 $mA{\cdot}cm^{-2}$ and long-term OER stability, which are mainly attributed to the enlarged electrochemical active surface area and accelerated charge-transfer rate in this unique structure.

The activity of MOFs in electrocatalytic oxygen evolution reactions is currently receiving increasing attention. In addition to its high catalytic performance, the structure-activity relationship (especially the active site) is still poorly understood. Zhao *et al.* reported that the $Ni_{0.5}Co_{0.5}$-MOF-74 catalyst was characterized and analyzed during the OER reaction[174]. The study found that the $Ni_{0.5}Co_{0.5}$-MOF-74 material creates higher defects and higher chemical valence *in situ* during the OER process, which is responsible for the higher OER performance of the catalyst. When the ratio of Ni and Co in the material is altered, the *in situ* generated active species in the catalyst changes in composition structure and electronic structure so that the catalytic activity is modulated. In addition, noble metals, which are expensive and less stable, have been used as catalysts for OER due to their high catalytic activity. To replace the noble metal catalyst, 3d transition metal-based materials, which are relatively inexpensive and have adequate catalytic activity, have been widely studied as promising candidates for OER catalysts. However, their moderate OER performance presents an obstacle to practical application. The introduction of oxygen vacancies is an effective way to tune the various properties of catalysts, which, in turn, can enhance the catalytic activity. Recently, Kang *et al.* reported a simple preparation strategy from MOFs to $Co(OH)_2$-Co_3O_4 hybrid catalysts with oxygen vacancies[175]. They found that the Co-based catalysts exhibited different morphology, composition and oxygen vacancy ratio to achieve higher activation catalytic performance by controlling the dosage of hexamethylenetetramine (HMT). As the results show, the heterogeneous $Co(OH)_2$-Co_3O_4 catalyst has excellent activity, with significantly higher OER performance at a current density of 10 $mA{\cdot}cm^{-2}$ and low overpotential of 280 mV. This strategy also expands new methods for preparing high oxygen vacancy ratio catalysts from MOFs.

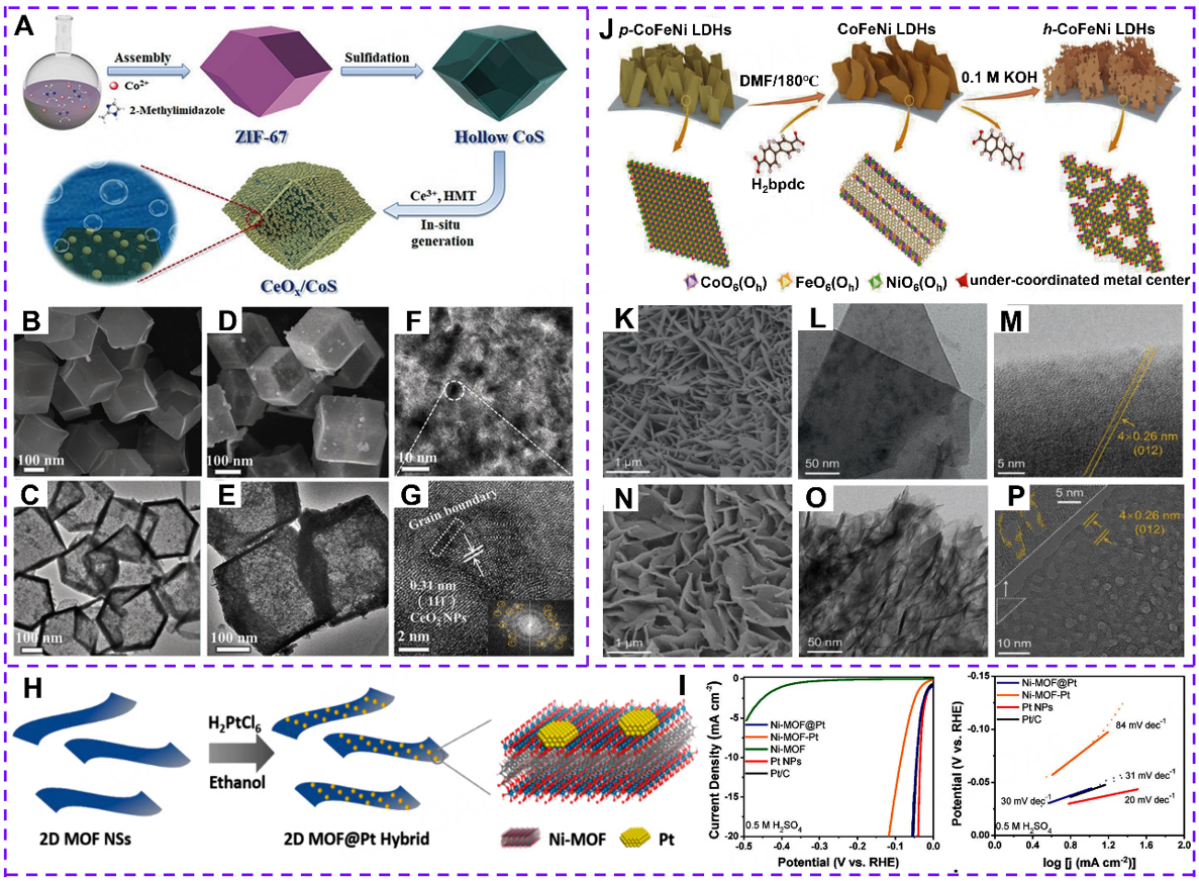

Figure 10. (A) Design synthesis strategy of CeO_x/CoS, (B and C) SEM and TEM images of CoS, (D-G) SEM and TEM images of CeO_x/CoS. Reproduced with permission[172]. Copyright 2018, Wiley-VCH. (H) Schematic diagram of Ni-MOF@Pt catalyst synthesis, (I) Performance of Ni-MOF@Pt catalyst HER. Reproduced with permission[179]. Copyright 2019, American Chemical Society. (J) The process for the preparation of porous CoFeNi-LDH catalyst, (K) SEM images of p-$Co_{0.34}Fe_{0.33}Ni_{0.33}$-LDH, (L) TEM images of p-$Co_{0.34}Fe_{0.33}Ni_{0.33}$-LDH, (M) HR-TEM images of p-$Co_{0.34}Fe_{0.33}Ni_{0.33}$-LDH, (N) SEM images of h-$Co_{0.34}Fe_{0.33}Ni_{0.33}$-LDH, (O) TEM images of h-$Co_{0.34}Fe_{0.33}Ni_{0.33}$-LDH, (P) HR-TEM images of h-$Co_{0.34}Fe_{0.33}Ni_{0.33}$-LDH. Reproduced with permission[181]. Copyright 2020, Wiley-VCH.

HER: HER catalysis is a significant step in the development of hydrogen energy, and worthwhile results have been achieved for strategies such as semiconductor-based photocatalysis, photocatalysis, and metal-based electrocatalysis[176-178]. However, it is still important to explore high-efficiency HER catalysts with high abundance and low price.

In recent years, MOF derivatives have been widely concerned by researchers for electrochemical applications due to their abundant defects, many active sites and diverse structures. For example, in 2019, Rui *et al.* reported on an efficient strategy for the rapid construction of noble metal/2D MOF heterostructures[179]. The method involves *in situ* growth of noble metal nanoparticles on the defect-rich surfaces of ultrathin MOF nanosheets [Figure 10H]. The 2D Ni-MOF@Pt composite catalysts with well-defined interfaces can be used for electrochemical HER. The Ni-MOF@Pt current densities of 241 $mA{\cdot}mg^{-1}$ at -100 mV in 1 M KOH and 126 $mA{\cdot}mg^{-1}$ at -35 mV in 0.5 M H_2SO_4 outperformed the pure Pt NPs (146 and 54 $mA{\cdot}mg^{-1}$) [Figure 10I]. It indicates that Ni-MOF@Pt has excellent catalytic activity under acid-base conditions.

Layered double hydroxide (LDH) is an excellent electrocatalyst for OER. However, its application in electrocatalytic hydrolysis is limited by the sluggish kinetics of the Volmer step of the HER in an alkaline medium. Currently, some researchers have successfully reduced the hydrolysis barrier by introducing Ru/Ir into LDH, thus achieving better HER performance[180]; however, the introduction of noble metals will undoubtedly increase the manufacturing cost of the catalyst. In 2020, Sun *et al.* used a simple strategy using MOF as a precursor for *in situ* topological structure transformation to prepare holey ternary CoFeNi-LDH catalysts on the surface of nickel foam [Figure 10J-P][181]. Such polygonal pores expose atomistic edge steps and lattice defects, forming a large number of unsaturated coordination metal centers, which, together with the modulation of the metal valence state by Fe, synergistically promote the hydrolysis kinetics of HER, ultimately obtaining excellent electrolytic water properties. The optimized catalysts exhibited overpotentials of 71 mV and 195 mV for HER and OER, respectively, which was superior to the Pt/C-RuO_2 combination. It also has excellent stability and can operate continuously for more than 25 h at a current density of 300 $mA{\cdot}cm^{-2}$. In addition, the ratio of different doping metals has a tremendous effect on the performance of the catalyst. Gopi *et al.* designed and synthesized Ni/Fe bimetallic catalysts with various molar ratios. It was demonstrated that when the molar ratio of Ni and Fe was 0.06:0.06, the catalysts exhibited excellent catalytic performance for both OER and HER in acidic and alkaline mediums[182]. In addition, vanadium doping effectively improved the OER and HER properties of Ni-Fe MOF/GO composites, while in vanadium doping, the defects on the MOF/GO surface contributed significantly to the corrosion potential of V-Ni_xFe_y-MOF/GO electrocatalysts. The electrocatalytic properties of typical defective MOFs and derivatives are summarized in Table 3.

ORR: The development of green and sustainable next-generation energy conversion technologies will have great significance in alleviating the energy crisis from environmental pollution. However, its core reaction ORR involves multi-step proton-electron coupling, and its reaction kinetics are very sluggish, which severely restricts the development of technologies such as fuel cells[183-185]. Currently, noble metal Pt-based catalysts exhibit the optimal ORR catalytic activity, but their scarcity in abundance and high prices make it difficult to spread their popularity[186,187]. Therefore, it is a significant challenge to develop novel ORR catalysts that are low-cost, environmentally friendly and high efficiency.

Single-atom catalysts have shown larger potential for application in many catalytic reaction systems due to their unsaturated coordination environment, highest atomic utilization, and unique electronic structure. In particular, the transition metal monoatomic catalysts loaded on carbon carriers have outstanding catalytic performance. In 2021, Yuan *et al.* proposed a strategy for constructing defect-rich MOF-derived single-atom catalysts by decarboxylation-induced effects for enhancing the electrocatalytic activity of transition metal Co-N_4 single-atom sites [Figure 11A][188]. The Zn-MOF (DMOF), which is rich in both carboxyl functional groups and nitrogen, was firstly constructed by the "mixed linker approach", and then the single-atom derivatization catalyst (Co@DMOF-900) was obtained by the gas-phase migration method using DMOF as the precursor and $CoCl_2$ as the Co source, realizing the simultaneous *in situ* construction of Co-N_4 single-atom sites and carbon framework defects. It is further demonstrated by a series of characterization techniques and theoretical calculation methods that carbon defects induced by decarboxylation can effectively enhance the activity of metal single-atom sites in the electrocatalytic ORR process. This is mainly attributed to the increased activity of the Co-N_4 active site in Co@DMOF catalysts with defect-rich carbon structure, with conversion frequency TOF and mass current density j_m up to 2.015 $e{\cdot}s^{-1}{\cdot}site^{-1}$ and 3.3 $A{\cdot}mg^{-1}$, respectively. In addition, defect-rich carbon materials are considered to be a class of highly active catalytic reaction sites with electrocatalytic properties comparable even to those of noble metal electrocatalysts. Recently, Wu *et al.* reported the use of Zn-MOF (ZIF-7) as a specific precursor to control the removal and reconstitution of carbon atoms through thermal redox reactions in the restricted

Table 3. A summary of the reported defective MOFs and their derivative as OER and HER electrocatalysts and their catalytic performance

Catalyst	Defects type	Current density (j, mA·cm^{-2})	Overpotentials (η) at corresponding (mV)	Applications	Reference
CeO_x/CoS	Vacancies	10	269	OER	[172]
CoCu-MOF	Vacancies	10	295	OER	[173]
$Ni_{0.9}Fe_{0.1}$-MOF	Vacancies	10/20	198/231	OER	[174]
$Co(OH)_2$-Co_3O_4	Vacancies	10	280	OER	[175]
Ni-MOF@Pt	Doping defects	10	43	HER	[179]
NiVRu-LDH	Vacancies	10	12	HER	[180]
h-$Co_{0.34}Fe_{0.33}Ni_{0.33}$-LDH	Vacancies	10	71	HER	[181]
V-$Ni_{0.06}Fe_{0.06}$ MOF/GO	Doping defects	10	90	HER	[182]

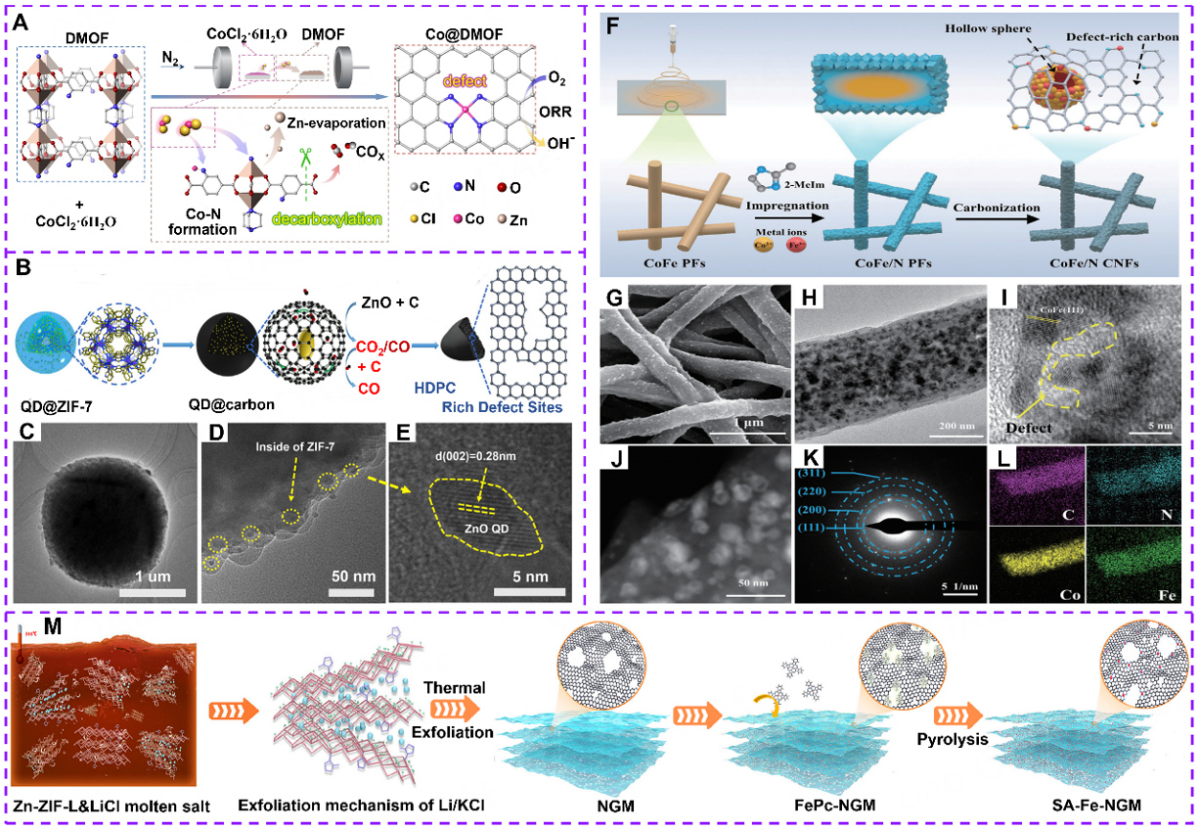

Figure 11. (A) Schematic illustration of MOFs decarboxylation-induced effect to construct defect-enhanced single-atom catalysts. Reproduced with permission[188]. Copyright 2021, Wiley-VCH. (B) Schematic illustration of the preparation of porous carbon with high defect density, (C) TEM image of ZnO@ZIF-7, (D and E) HRTEM image of ZnO quantum dots encapsulated by ZIF-7. Reproduced with permission[189]. Copyright 2022, Elsevier. (F) Schematic illustration of the preparation of CoFe/N CNFs, (G and H) SEM image (I) TEM image, (J) HAADF-STEM image, (K) SAED pattern, (L) EDS mapping of CoFe/N CNFs. Reproduced with permission[190]. Copyright 2022, Springer. (M) Schematic illustration of the synthesis process of SA-Fe-NGM. Reproduced with permission[191]. Copyright 2022, American Chemical Society.

ZIF-7 carbon cavity with ZnO quantum dots and the generation of CO_2 gas [Figure 11B][189]. The resulting porous carbon contains ultra-high density carbon defects (HDPC) with densities up to 2.46 × 10^{13} cm^{-2} (The structure is characterized as shown in Figure 11C-E). When applied to oxygen reduction reactions, the porous carbon has excellent catalytic properties in both alkaline and acidic medium, with half-wave

potentials of 0.90 or 0.75 V at 0.1 M KOH or $HClO_4$, respectively. Furthermore, the normalized specific activity and density functional theory calculation reveal a gradient "proximity effect" between carbon defects with different spatial distance, indicating that the quantitative control of carbon defect density is the key to enhancing electrocatalytic activity.

Moreover, Chen *et al.* developed a novel fabrication method to construct 3D unique defect-rich electrocatalysts in which irregular hollow CoFe nanospheres are embedded in N-doped carbon nanofibers (CoFe/N CNF) [Figure 11F], the morphology, elemental and structural information of CoFe/N CNFs are shown in Figure 11G-L[190]. The diameter of the optimized CoFe-ZIF is about 25 nm, which provides enriched active sites. The defect-rich carbon and irregular hollow CoFe nanospheres exhibited superior catalytic activity under 10 $mA{\cdot}cm^{-2}$ in alkaline media with a potential difference of only 0.67 V between OER potential and ORR half-wave potential, which is comparable to commercial catalysts with 20% Pt/C and RuO_2 blends. In addition, MOFs are regarded as ideal precursors for the synthesis of Fe single-atom catalysts. However, most MOF-derived catalysts have 3D morphology, resulting in numerous Fe-N_x catalytic active sites buried inside the catalyst particles, which cannot directly participate in the reaction. Therefore, it is necessary to construct catalyst morphologies with high exposure of Fe-N_x active sites and combine them with mesoporous channels to promote the utilization of active sites. Li *et al.* have adopted an exfoliation strategy to firstly exfoliate Zn ZIF-containing nanosheets into ultrathin two-dimensional graphene nanonetworks (NGM) employing KCl and LiCl as exfoliating as well as etching agents, and secondly obtain hierarchical porous structures with desired pore sizes by regulating the ratio of LiCl to KCl, and eventually selected as a precursor for the formation of Fe-N_x active sites by high-temperature pyrolysis of FePc to obtain the Fe-single-atom catalysts (SA-Fe-NGM) [Figure 11M][191]. Furthermore, The SA-Fe-NGM is found to deliver a superior oxygen reduction reaction (ORR) activity in acidic media (half-wave potential = 0.83 V *vs.* RHE) and a high-power density of 634 $mW{\cdot}cm^{-2}$ in the H_2/O_2 fuel cell test.

CO_2RR: The appropriate number of defects can modify the local properties of a solid material and enhance its performance. Therefore, regulating the electronic and geometric structure of MOF catalysts by defect engineering to improve electrocatalytic CO_2 reduction activity is a very effective strategy.

Heteroatom-doped materials are widely used in electrocatalytic CO_2 reduction by modulating the absorption/desorption of reaction intermediates through the electronic properties and chemical reactivity of carbon materials. For example, recently, Ling *et al.* developed a K^+-assisted synthesis strategy that utilizes freely movable dimethylammonium cations ($MeNH^{2+}$) within the one-dimensional pores of the electronegative framework material bio-MOF-1 to replace $MeNH^{2+}$ within the pores with K^+ *via* an ion-exchange strategy to obtain K^+@bio-MOF-1 materials[192]. The final defective carbon material K-defect-C-1100 with a single carbon defect center-vacancy type V_{12} (missing 12 near-neighboring carbon atoms at the defect) was obtained by high-temperature pyrolysis of K^+@bio-MOF-1 material [Figure 12A]. Unexpectedly, K-defect-C generated CO by CO_2 electroreduction at -0.45 V with a Faraday conversion efficiency of 99% [Figure 12B and C], far exceeding that of MOF-derived carbon without K^+ etching. In addition, single-atom sites are also considered promising catalytic modulators. However, in electrochemical CO_2RR reaction systems, the introduction of single atoms triggers a competitive HER, which leads to a decrease in CO_2RR product selectivity. Hu *et al.* proposed a bimetallic single-atom catalyst strategy consisting of transition metal and main group metal sites. The mesoporous N-doped carbon-anchored Cu/In bimetallic site catalysts (Cu-In-NC) were prepared by pyrolysis of Cu and In co-doped ZIF-8 (Cu-In-ZIF-8) under argon atmosphere [Figure 12D][193]. During thermal conversion, a large number of defective sites on Cu-In-ZIF-8 further expand to form mesopores [Figure 12E and F]. The formation of mesopores can improve the catalyst mass transfer efficiency and thus enhance the accessibility of the active center. In CO_2RR, the HER

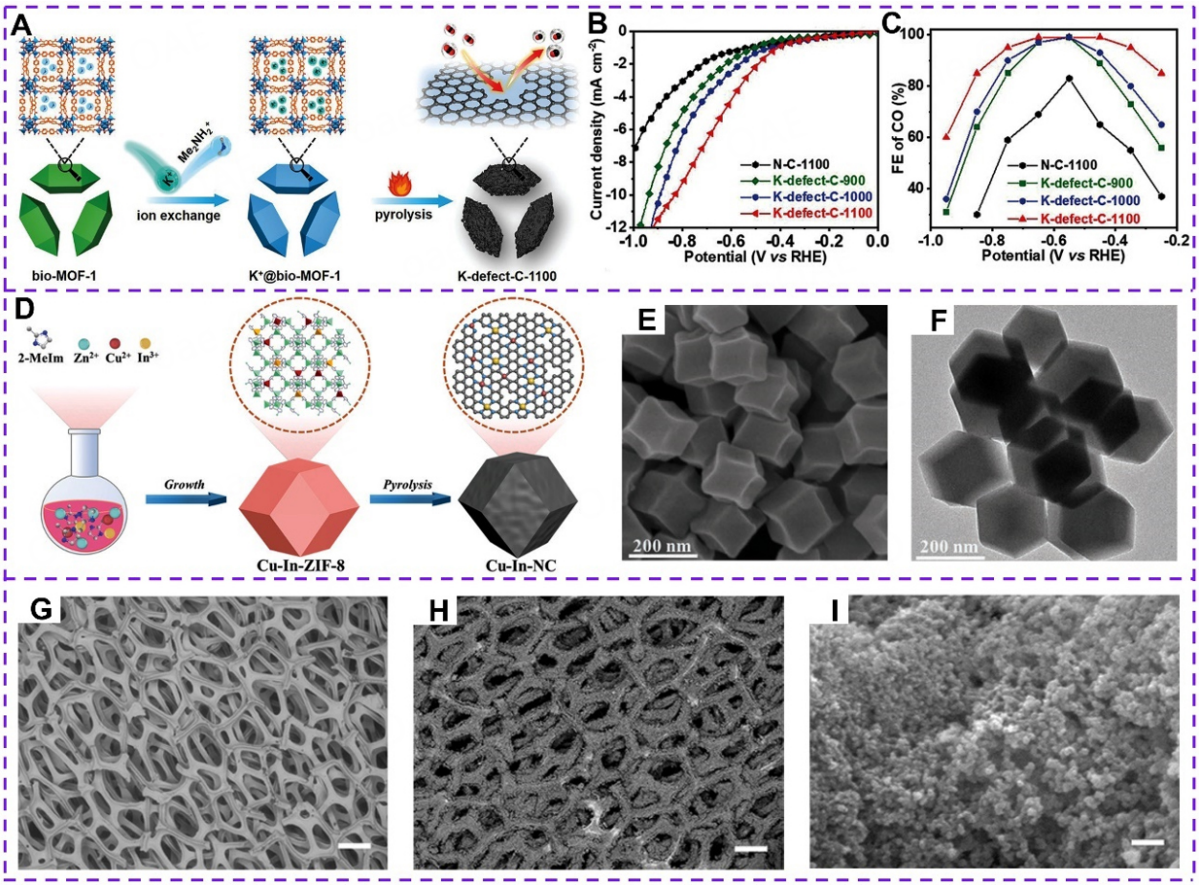

Figure 12. (A) Schematic illustration of K^+-assisted construction of intrinsically defective carbon material, (B) LSV curves, (C) FEs of CO at different applied potentials. Reproduced with permission[192]. Copyright 2022, Wiley-VCH. (D) Cu-In-NC preparation schematic, (E) SEM image of Cu-In-ZIF-8, (F) TEM image of Cu-In-ZIF-8. Reproduced with permission[193]. Copyright 2022, Wiley-VCH. (G) SEM image of Cu-foam electrode, (H and I) SEM images of Cu_2(L)-e/Cu. Reproduced with permission[194]. Copyright 2020, Springer Nature.

inert in site substantially enhances the performance of the Cu site for CO_2 reduction. The CO faradic efficiency FE CO of Cu-In-NC reaches 96% at -0.7 V, which is significantly better than that of Cu-NC (55% for FE CO) and In-NC (54% for FE CO).

Moreover, MOF compounds with infinite metal sites and pore structures have promising potential in the field of electrochemical CO_2 reduction. The metal centers can be used as active catalytic sites, and the porosity facilitates the adsorption of CO_2. In 2020, Kang *et al.* invented the method of modifying Cu-MOF with high defective sites on Cu foam [Figure 12G][194]. By selecting ligands with a high spatial site resistance, the Cu-MOF with more defects on the surface of Cu foam was rapidly modified using electrochemical growth methods. The EPR analysis shows that the Cu-MOF obtained by electrochemical growth has 15.3% Cu^{2+} defect sites, while the Cu-MOF obtained by the conventional thermal synthesis method contains only 1.5% Cu^{2+} defect sites [Figure 12H and I]. Meanwhile, the Cu-MOF/Cu electrode in acetonitrile electrolyte produced a current density of 65.8 mA·cm^{-2} at -1.8 V *vs.* Ag/Ag$^+$ with a formic acid Faraday efficiency of 90.5%. Compared with the single metal catalyst, the performance improvement of bimetallic catalysts is mainly attributed to the multiple factors among structure, interface, and various synergistic effects resulting from the coupling of two metals. For the rational design of Cu-based bimetallic catalysts and understand the promotion mechanism between Cu-based bimetallic catalysts on CO_2 reduction. In 2019, Albo *et al.* reported the performance of Cu(II) and Bi(III)-based metal-organic framework (HKUST-1 and CAU-17,

respectively) blends into the electroreduction of CO_2 to alcohols in a filter-press electrochemical cell[195]. The results revealed a synergic effect of Cu and Bi-based MOFs, associated with a favored interplay between the actives sites and reaction intermediates, prompting methanol formation and C-C coupling reaction to ethanol. The optimum values for a more selective CO_2 reduction to alcohols can be set at a Bi content of 12% and a acurrent density of j = 20 mA·cm^{-2}. Similarly, Albo *et al.* synthesized four MOPMs (HKUST-1, CuAdeAce, CuDTA and CuZnDTA) containing Cu as gas diffusion electrodes[196]. The electrodes show relatively high surface areas, accessibilities, and exposure of the Cu catalytic centers as well as favorable electrocatalytic CO_2 reduction performance. The maximum cumulative Faradaic efficiencies for CO_2 conversion at HKUST-1, CuAdeAce, CuDTA, and CuZnDTA based electrodes are 15.9, 1.2, 6, and 9.9%, respectively, at a current density of 10 mA·cm^{-2}, an electrolyte-flow/area ratio of 3 mL·min·cm^{-2}, and a gas-flow/area ratio of 20 mL·min·cm^{-2}.

Others

It has long been important that defects in crystalline materials are controlled as they are related to the properties of the material. Ye *et al.* have synthesized defective UiO-66, which has shown excellent catalytic activity in the oxidative desulfurization reactions of dibenzothiophene (DBT) and 4,6-dimethyldibenzothiophene (4,6-DMDBT)[197]. They synthesized UiO-66-free and UiO-66-solvent with 2.16 and 1.53 linkers missing per unit cell, respectively, where the higher degree of defective UiO-66-free could improve the removal of DBT up to 99.6%, while the corresponding value of UiO-66-solvent was 80.5%. More surprisingly, the difference between UiO-66-free and UiO-66-solvent for 4,6-DMDBT removal was even greater, 98.1% and 52.5%, respectively. Recently, Xu *et al.* used defect design strategies to introduce two types of defects into the MIL-100-Cr framework[198]. Meanwhile, Ru NPs with defective sites anchoring the restricted domains were used to achieve the Ru-loaded DEMOF catalysts (Ru@DEMOF), and the obtained Ru@DEMOF catalysts simultaneously enhanced the activity and cycling stability of the reaction for the selective hydrogenation of glucose to prepare sorbitol.

Electrochemical energy storage

Defect engineering was available to tune the morphology and structure of the MOF. The removal of linkers or clusters by coordination bond breaks results in the formation of defects in the MOF structure with missing links or clusters, thus its adjustment of electronic structure and optimization of properties[199-201]. Therefore, in the design of electrode materials, the number of active sites of catalysts can be increased, the utilization rate of active sites can be improved, and the structural stability can be optimized by defect engineering, so that efficient and stable metal-based batteries can be designed[202-204]. These defective MOFs are highly active and are used in energy storage for a wide range of applications, including LIBs, ZIBs, Li-S, and other batteries[205,206]. In this section, we summarize the recent advances in energy storage based on defective MOFs and their derivatives (summarized in Table 4).

Lithium-ion batteries

With the benefits of superior energy density and lower environmental pollution, LIBs stand out among many energy storage devices and have received more and more attention from researchers[207-210]. Further improvement of electrochemical energy storage in LIBs is urgent due to the limited conductivity and theoretical capacity of conventional electrode materials[211,212]. However, the simplest way to solve this problem is to synthesize new electrode materials. In recent years, the MOFs aroused a lot of attention due to their unique structures. In particular, the introduction of the defect in the MOF structure will maximize the exposure of the metal active site, which has many advantages as an electrode material[213].

Table 4. Defective MOFs and their derivative materials for electrochemical energy storage performance

Material	Defects type	Performance	Applications	Reference
TiO_2/C nanocomposite	Vacancies	Reversible capacity (316.9 mAh·g^{-1} at 0.5 A·g^{-1}), rate capability (186.1 mAh·g^{-1} at 10 A·g^{-1}) and long cycle life (219.3 mAh·g^{-1} after 2,500 cycles at 5 A·g^{-1})	LIBs	[214]
Zn-Mn-MOF-derived O_V-ZMOs	Vacancies	At a current of 0.1 A·g^{-1}, the initial charge/discharge capacities of BDC-OV-ZMO, BTC- OV-ZMO and IN- OV-ZMO were 637.5/993 mAh·g^{-1}, 836.9/1313.6 mAh·g^{-1} and 479.9/750.8 mAh·g^{-1}, corresponding to coulometric efficiencies of 64.2%, 63.7% and 63.9%.	LIBs	[215]
MOF-CeO_2@Zn	Doping defects	Capacity of 282 mAh·g^{-1} after 600 cycles at 1 A·g^{-1} and a capacity of 97 mAh·g^{-1} at 20 A·g^{-1}	ZIBs	[219]
MnV_2O_4(p)/C-700	Doping defects	Capacity of 410 mAh·g^{-1} at 0.1 A·g^{-1} and energy density of 288.1 Wh·kg^{-1}, capacity retention is 94.3% after 1000 discharge/charge cycles at 20 A·g^{-1}.	ZIBs	[220]
MOF-derived MnO/C hybrids	Vacancies	Specific capacity with 336.8 mAh·g^{-1} at 0.1 A·g^{-1} and stability with 73.8% after 10,000 long cycles at 1.0 A·g^{-1}.	ZIBs	[221]
D-TiO_2@Gr	Doping defects	Specific discharge capacity of 1,049.3 mAh·g^{-1} after 100 cycles at 1C with a sulfur loading of 3.2 mg·cm^{-2}.	Li-S	[229]
D-UiO-66-NH_2-4	Doping defects	Initial capacity of 756 mAh·g^{-1} and corresponds to 92% retention after 600 cycles.	Li-S	[230]
aMIL-88B	Doping defects	Capacity retention of 740 mAh·g^{-1} after 500 cycles at 1 C, rate up to 5 C, and sulfur loading of 4.3 mg·cm^{-2}.	Li-S	[231]
S/ZIF-7 600	Doping defects	Initial capacities of 1,206.3 and 972.8 mAh·g^{-1} after 100 cycles at 0.2 C	Li-S	[232]
BHZ-48	Vacancies	Charge-discharge voltage gap of 0.8 V and a stable cyclability over 1,250 h are achieved at 15 mA·cm^{-2}	ZABs	[233]
Fe-NiCo-S nanosheet	Vacancies	Capacitance (2,779.6 F·g^{-1} at 1 A·g^{-1}) and rate (1,627.2 F·g^{-1} at 10 A· g^{-1})	SCs	[234]
Co-10/MCu-BTC	Doping defects	Capacities (7,123 mAh·g_{Cat+C}^{-1} for discharging and 7,662 mAh·g_{Cat+C}^{-1} for charging)	Li-air battery	[235]

Recently, there has been an increasing interest in plasma technology for tuning the properties of electrode materials. Many beneficial effects can be created through strong interactions among charged particles on the electrode materials. For example, in 2021, Sun *et al.* proposed the strategy of combining MOF-derived nano/micro structure and plasma fabrication to prepare TiO_2/C nanocomposites with high defect concentrations [Figure 13A-D][214]. The composite exhibits excellent electrochemical properties with a reversible capacity of 316.9 mAh·g^{-1} at 0.5 A·g^{-1} and possesses a high-rate capacity of 186.1 mAh·g^{-1} at 10 A·g^{-1}. The reason can be attributed to the fact that the energetic ion bombardment not only increases the specific surface area and active sites of the material, but also introduces a high concentration of defects. More importantly, the introduction of oxygen vacancies, Ti^{3+} ion and lattice distortion can improve the intrinsic conductivities, which is also verified by density functional theory calculations as well as the resistivity and GITT measurements. In addition to composite materials, MOF-derived materials are also used in lithium-ion battery electrode materials. Recently, Lin *et al.* used different Zn-Mn based MOFs as

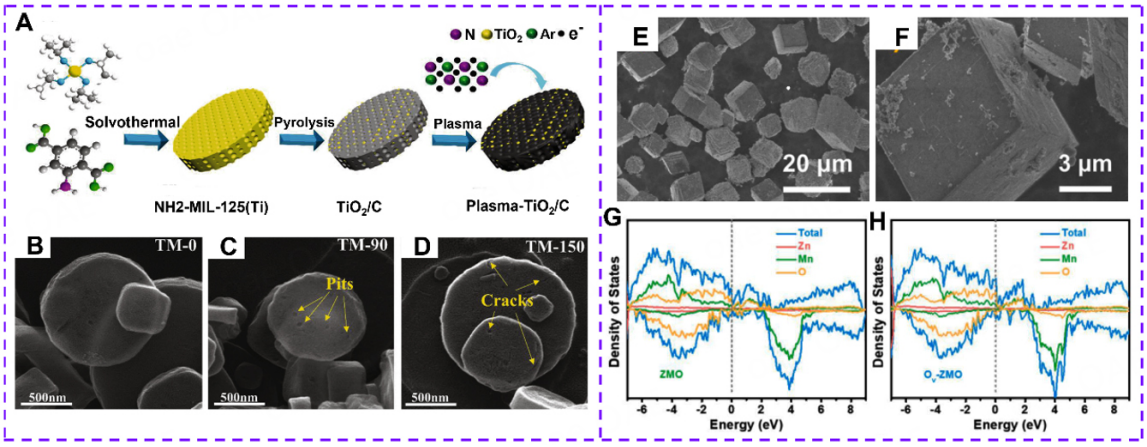

Figure 13. (A) Schematic illustration of the preparation of plasma TiO_2/C, SEM images of TiO_2/C with different plasma power; (B) TM-0; (C) TM-90; (D) TM-150. Reproduced with permission[214]. Copyright 2021, Elsevier. (E and F) SEM images of BDC-O_V-ZMO, TDOS and PDOS profiles of (G) ZMO and (H) O_V-ZMO. Reproduced with permission[215]. Copyright 2022, Elsevier.

precursors to construct anode materials of oxygen vacancy-rich $ZnMn_2O_4$ and obtained excellent specific capacity and rate performance, effectively improving the electrochemical performance of $ZnMn_2O_4$ from the atomic level[215]. The constant current charge/discharge test at 0.1 $A{\cdot}g^{-1}$ confirmed the excellent specific capacities of BDC-O_V-ZMO [Figure 13E and F], BTC- O_V-ZMO and IN- O_V-ZMO (initial charge/discharge capacities of 637.5/993 $mAh{\cdot}g^{-1}$, 836.9/1313.6 $mAh{\cdot}g^{-1}$ and 479.9/750.8 $mAh{\cdot}g^{-1}$, respectively). In addition, DFT calculations can further explain the effect of abundant oxygen vacancies on the lithium storage capacity of ZMO anode materials [Figure 13G and H] mechanistically.

Zinc-ion batteries

In recent years, the aqueous ZIBs have received a lot of attention from researchers because of their environmental friendliness, safety and economic advantages[216,217]. However, ZIBs still face some problems, such as the dissolution and collapse of electrode materials leading to poor full cell cycling performance; the strong electrostatic attraction between divalent Zn ions and host atoms leading to poor rate performance of the full cell[218]. Therefore, it is significant to find suitable electrode materials for developing high-performance ZIBs.

Recently, Li *et al.* proposed the smart artificial SEI by calcination of MOF precursors to derive porous CeO_2 with abundant defects (MOF-CeO_2@Zn) as zinc anodes to enhance the cycle life of batteries [Figure 14A][219]. The crystal defects in MOF-CeO_2 can provide abundant active sites for the transfer of Zn ions, which can accelerate the transport of Zn ions [Figure 14B-E]. At the same time, this porous structure balances the ion flux and combines with an inhibition of the solvation effect, leading to a uniform deposition of Zn and suppressing the formation of Zn dendrites. As a result, the MOF-CeO_2@Zn anode exhibits an ultra-stable plating/stripping behavior (over 3,200 h) and high coulometric efficiency (99.5% coulometric efficiency at 2 $mA{\cdot}cm^{-2}$). In addition, this multifunctional protective layer improves significantly the overall performance of the Zn||MnVO full cell, which still has a specific capacity of 163 $mAh{\cdot}g^{-1}$ after 10,000 cycles at 5 $A{\cdot}g^{-1}$. Leng *et al.* were the first to design and synthesize oxygen-rich defective MOF-derived MnV_2O_4/C materials to be used in aqueous zinc ion batteries[220]. They selected two MOF precursors, $[Mn(phen)H_2O][V_2O_6]$ and $[Mn(bpy)\ V_2O_6]$-$1.16H_2O$, to investigate the effects of the type of Mn-V MOF precursor and calcination temperature on the electrochemical behavior of the resulting MnV_2O_4/C composites [Figure 14F and G]. The optimal sample MnV_2O_4(p)/C-700 exhibited a capacity retention rate of 94.3% after 1000 charges/discharges at 20 $A{\cdot}g^{-1}$ [Figure 14H]. Ex situ X-ray diffraction,

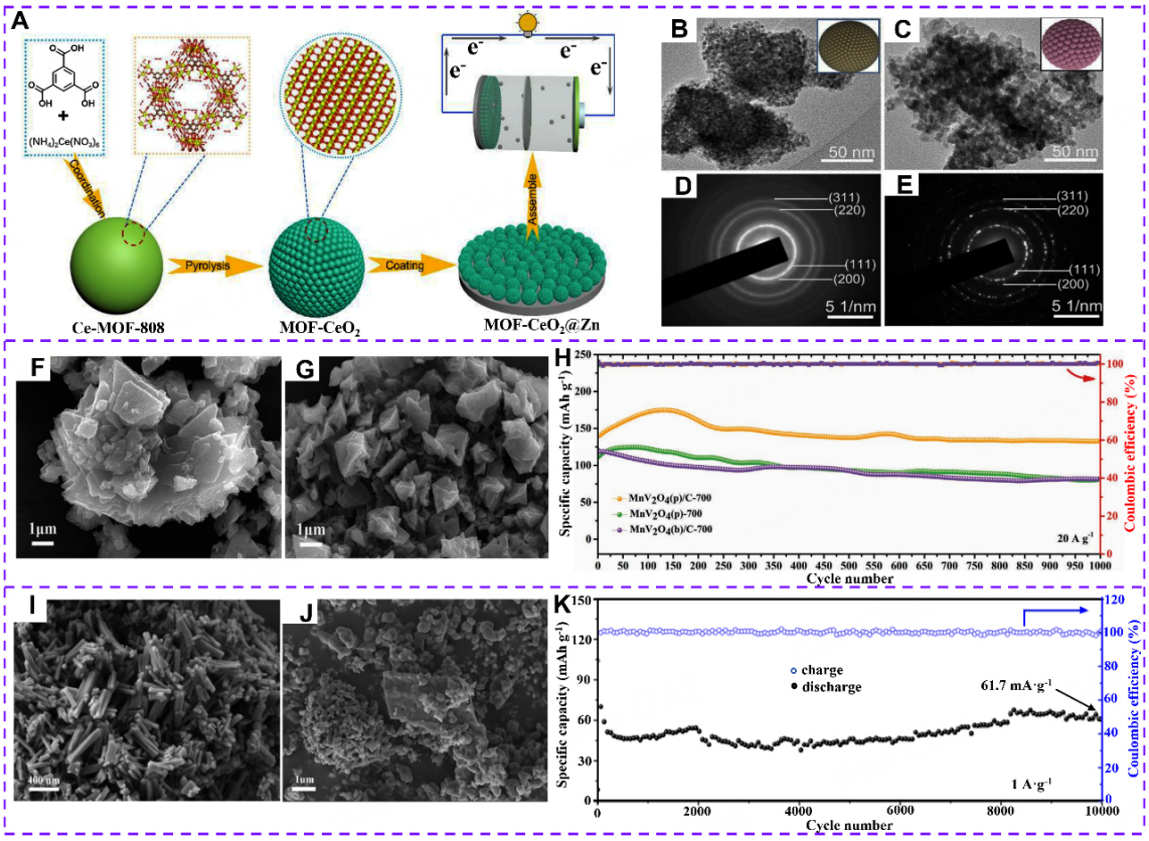

Figure 14. (A) Schematic illustration of the synthesis of MOF-CeO_2 and the foil coating process in Zn, (B) SEM images of MOF-CeO_2/C, (C) SEM images of MOF-CeO_2 (D) SEAD analysis of MOF-CeO_2/C, (E) SEAD analysis of MOF-CeO_2. Reproduced with permission[219]. Copyright 2023, Elsevier. (F) SEM images of MnV_2O_4(p)-700, (G) SEM images of MnV_2O_4(p)/C-700, (H) long-term cycle life of MnV_2O_4(p)/C-700. Reproduced with permission[220]. Copyright 2021, Wiley-VCH. (I) SEM images of Mn-BTC, (J) SEM images of 700-Air, (K) long-term cycling performance of 700-Ar. Reproduced with permission[221]. Copyright 2022, Elsevier.

scanning electron microscopy, energy-dispersive X-ray spectra, as well as elemental mappings and X-ray photoelectron spectroscopy of MnV_2O_4(p)/C-700 discern the partial phase transformation mechanism of $MnV_2O_4 \rightarrow Zn_3(OH)_2V_2O_7(H_2O)_2$ during discharge/charge process. Sun *et al.* adopted a similar method to prepare a MnO/C hybrid material derived from Mn-BTC and rich in oxygen vacancies [Figure 14I and J][221]. The effect of air and argon on the formation of oxygen vacancies was investigated. The incorporation of oxygen vacancies can tune the electronic rearrangement and crystal microstructure via the different calcination atmospheres of air (Mn_2O_3) and Ar (MnO/C). Furthermore, the oxygen vacancy can effectively promote the reaction kinetics and electrochemical performance of manganese-based oxide hybrids. Meanwhile, the oxygen vacancy-enriched MnO/C, with a specific capacity of 336.8 mAh·g^{-1} at 0.1 A·g^{-1}, exhibits excellent stability in long-cycle tests with 73.8% capacity retention over up to 10,000 cycles [Figure 14K].

Lithium-sulfur batteries

Lithium-sulfur batteries (Li-S) have been considered as one of the most promising devices for energy storage attributed to their ultra-high energy density (2,567 Wh·kg^{-1}) and theoretical capacity (1,675 mAh·kg^{-1})[222-224]. However, the sluggish reaction kinetics and shuttle effect of the reaction intermediate lithium polysulfide have hindered the relevance of Li-S for practical applications[225,226]. The preparation of anode carrier materials that can anchor lithium polysulfide is the simplest and most effective

main method to solve the shuttle problem. Meanwhile, defect engineering is widely used to synthesis functional materials with electron-rich active sites[227,228]. It is reported that many defect-engineered materials are superior to defect-free materials in accelerating polysulfide conversion. Therefore, it is significant to apply defect engineering to the conversion of lithium polysulfides to enhance the performance of Li-S.

In order to demonstrate that defects in the cathode host material of Li-S can be effective in their performance. In 2020, He *et al.* reported a study of the oxygen-deficient sulfur-containing material TiO_2 (D-TiO_2) using DFT calculations[229]. Based on the results of DFT calculations, the composite structure of 3D graphene aerogel containing oxygen defective TiO_2 (D-TiO_2@Gr) as an anode carrier was reconstructed. Electrochemical performance tests showed that the 3D graphene aerogel (D-TiO_2@Gr) composite of D-TiO_2 was proved to be an excellent sulfur host and the specific discharge capacity was 1,049.3 mAh·g^{-1} with a sulfur loading of 3.2 mg·cm^{-2} after 100 cycles at 1C. Even with the sulfur mass loading increasing to 13.7 mg·cm^{-2}, an impressive stable cycling is obtained with an initial areal capacity of 14.6 mAh·cm^{-2}, confirming the effective enhancement of electrochemical performance by the oxygen defects. Li *et al.* proposed the construction of defective UiO-66-NH_2-4/graphene electrocatalytic membrane (D-UiO-66-NH_2-4/G EM) [Figure 15A] by defect engineering strategy to achieve the excellent electrochemical performance of Li-S under the harsh conditions of high sulfur loading and low electrolyte/sulfur ratio[230]. Their research revealed that the D-UiO-66-NH_2-4 framework effectively suppresses the shuttle effect through Lewis acid-base interaction between UiO(Zr) and polysulfides, provides sufficient sites for capturing polysulfides through strong chemical affinity interactions, and provides active sites for efficiently converting polysulfides with effective electrocatalytic activity. Most importantly, a Li-S battery with such an electrocatalytic membrane delivers a high capacity of 12.3 mAh·cm^{-2} (1,013 mAh·g^{-1}) at a sulfur loading up to 12.2 mg·S·cm^{-2} under a lean electrolyte condition (E/S = 5 μL·mg^{-1}-sulfur) at 2.1 mA·cm^{-2} (0.1 C). In 2021, Zhang *et al.* synthesized amorphous MIL-88B (aMIL-88B) by a simple ligand competition method[231] [Figure 15B]. SEM images revealed that the surface of aMIL-88B was rougher compared to that of cMIL-88B and was also accompanied by the appearance of some cracks, which could be confirmed by TEM images. Meanwhile, the direct immersion of crystalline MIL-88B (denoted as cMIL-88B) in dimethylimidazole solution triggers the partial substitution of amino terephthalate by 2-Methylimidazole (2-MeIM), followed by the hydroxylation that leaves the deficiency of organic ligand at these sites. Such amorphization endows the aMIL-88B [Figure 15C-E] with higher electrochemical performance, more active sites exposure, and higher adsorptive/catalytic activity to polysulfides compared with those of the parent MIL-88B counterpart. Therefore, Li-S batteries with the as-developed amorphous MOF (aMIL-88B)-modified separator realize efficient and reversible sulfur electrochemistry, exhibiting superb cyclability with high-capacity retention of 740 mAh·g^{-1} after 500 cycles at 1 C, rate performance up to 5 C, and also decent areal capacity under a high sulfur loading of 4.3 mg·cm^{-2}. Recently, Wang *et al.* used thermal treatment to prepare porous 2D defective ZIF-7 with abundant active edges for application as sulfur carriers in Li-S[232]. The 2D porous defective MOF (ZIF-7) was obtained by etching and creating pores through a simple thermal treatment. [Figure 15F] It was found that the ZIF-7 600 material obtained at a calcination temperature of 600 had the largest specific surface area as well as the largest sulfur loading, demonstrating the enormous potential of ZIF-7 600 [Figure 15G and H] as a sulfur carrier. As a result, the synthesized ZIF-7 600 for Li-S host material significantly improved the performance of Li-S, that is, exhibited high initial capacities of 1,206.3 and 972.8 mAh·g^{-1} after 100 cycles at 0.2 C.

Other batteries

The defective MOFs are also commonly used in other batteries besides those mentioned above, and the continuous efforts of researchers have reported numerous batteries with excellent performance.

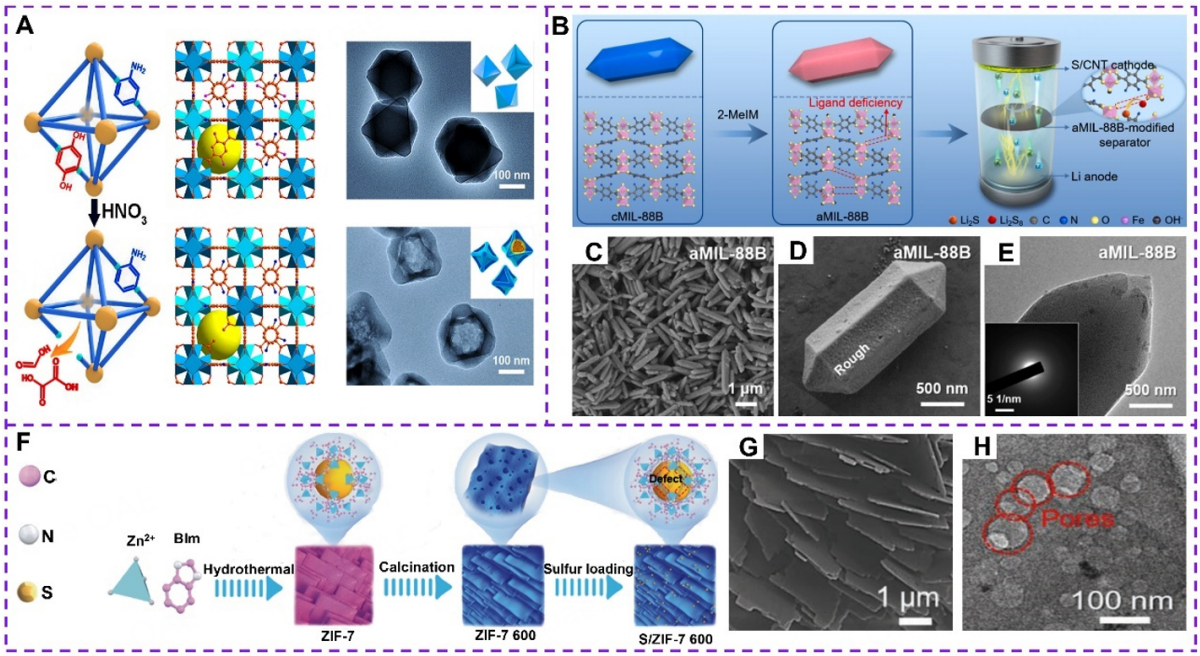

Figure 15. (A) Schematic illustration of D-UiO-66-NH_2 and TEM images. Reproduced with permission[230]. Copyright 2021, American Chemical Society. (B) Schematic illustration of the synthesis of amorphous aMIL-88B and its applications, (C and D) SEM images of aMIL-88B, (E) TEM images of aMIL-88B. Reproduced with permission[231]. Copyright 2021, Elsevier. (F) Schematic illustration of S/ZIF-7 600 synthesis, (G) SEM images of ZIF-7 600, (H) TEM images of ZIF-7 600. Reproduced with permission[232]. Copyright 2022, Wiley-VCH.

Zinc-air batteries (ZABs) are considered one of the most promising alternatives to LIBs due to their high energy density (1,086 $Wh{\cdot}kg^{-1}$), low cost, safety and environmental protection. Jiang *et al.* proposed the first innovative idea of using organic-inorganic hybrid materials by simultaneously introducing ligand vacancies and hierarchical pores into a heterometal imidazole framework to improve the performance of rechargeable zinc-air batteries[233]. Synchrotron radiation absorption spectroscopy and DFT modeling were used to investigate the origin of the active site in depth. Regulation of the *d*-orbital electronic structure of the active site metal Co by proximity interactions of ligand vacancies and long-range interactions of the cobalt-zinc alliance. Among the prepared series of materials, BHZ-48 has the optimal adsorption/desorption energy state of the active intermediate, and therefore the energy barrier of its potential decisive step is significantly reduced. Among the prepared series of materials, BHZ-48 has the adsorption/desorption energy state of the optimal active intermediate so that the energy barrier of its potential decision step is significantly reduced, which can lead to higher energy density and cycle life of ZABs. Liu *et al.* proposed the introduction of Fe-dopants and S vacancies into MOFs-derived bimetallic nickel-cobalt sulfide composites using a two-step solvothermal method to prepare Fe-NiCo-S samples with excellent charge storage kinetics and activity, and the obtained Fe-NiCo-S nanosheets have ultra-high specific capacitance (2,779.6 $F{\cdot}g^{-1}$ at 1 $A{\cdot}g^{-1}$) and excellent rate performance (1,627.2 $F{\cdot}g^{-1}$ at 10 $A{\cdot}g^{-1}$)[234]. Additionally, based on the density functional theory (DFT) calculation, defects cause more electrons to appear near the Fermi level, which is conducive to electron transfer in electrochemical processes. Wang *et al.* developed a method for partial removal of coordination functional groups to introduce isophthalic acid during the coordination of Cu ions with 1,3,5-bezenetricarboxylic acid, which resulted in the construction of numerous mesoporous defects as well as Cu metal centers with unsaturated coordination in microporous Cu-MOF[235]. Experimental and theoretical calculations have shown that a large number of mesopores and unsaturated coordination of Cu metal centers can effectively reduce the spatial site resistance during the electrocatalytic process, thus enhancing

mass transfer, lowering the electron conduction resistance, improving the affinity with the reactants, and at the same time providing more storage space for Li_2O_2, the discharge product of insoluble Li-air batteries. In addition, after loading Co on mesoporous Cu-MOF, the most optimized catalyst can produce a discharge capacity of nearly 7,000 $mAh \cdot g^{-1}$ in Li-air batteries.

CONCLUSION AND OUTLOOK

All in all, this review summarizes the recent advances in defective MOF types, synthesis, and in their electrochemical applications. Defective MOFs have been widely studied as one of the most promising electrode materials in the past few years due to their abundant active sites, controllable defect degree, unique physicochemical properties (such as electronic band structures, electrical conductivity, and mechanical stability), and simple synthesis methods. The chemical nature of the defects formed during the synthesis of MOFs is closely related to the type and number of modulators used. In addition, the prepared defective MOFs not only retained the framework structure of the parent MOF but also exposed more active sites. As a result, linker missing, cluster missing and macroscopic defective MOFs were synthesized using various preparation methods and rigorous regulation strategies, and the obtained defective MOFs exhibited excellent electrochemical properties. This makes the defective MOFs beneficial for energy conversion and has potential application value in energy storage.

Based on this, this review presents the recent research progress of defective MOFs, including the types of materials, synthesis methods and their applications in the field of electrochemistry. Although defective MOFs have become one of the most popular research topics over the years owing to their unique structural advantages, and some enormous research progress has been made, their future development still faces many issues and challenges.

(1) Precise control of the type and distribution of defects. Although regulating the type and distribution of defects can maintain the stability of MOFs to a certain extent, precise control of the type and distribution of defects is still a thorny problem. If precise regulation of defect formation can be achieved in the coming years, not only the stability of MOFs can be maintained, but also the location of active site generation can be regulated to optimize the electrochemical properties of MOFs further.

(2) Advanced characterization methods and theoretical calculations: In order to study the effect of defect on the energy conversion/storage of MOFs systematically, it is necessary to explore and develop more advanced methods that can help us to study the effect of defect in the energy conversion/storage of MOFs dynamically.

(3) Understand the reaction mechanism of energy conversion and energy storage. For energy conversion, the active sites of defective MOFs are difficult to identify. For energy storage, there is an urgent need to determine the degree of defects in defected MOF materials to achieve optimal performance such as redox-active centers, safety, and cycling stability.

(4) Enhanced synergistic effects. Defects may enhance one aspect of the performance of MOFs while leading to the weakening of other properties. Future research is needed to optimize the synergistic enhancement of their multifaceted properties, such as the simultaneous enhancement of energy storage and catalytic properties of MOFs, to make them more effective for electrochemical applications.

(5) Stability of defects. Although different defects in energy storage and conversion processes show excellent stability, the introduction of defects may also affect the stability of MOFs, and future efforts are needed to optimize the synthesis methods to maintain the high stability of MOFs while introducing defects, which will significantly expand the application prospects of MOFs once they can function in a highly stable manner under complex environments.

Overall, defective MOFs have more structural advantages than traditional porous materials and exhibit better electrochemical performance in the energy storage/conversion fields. As the continuous progress of electrochemical research, it will gradually overcome and solve some existing problems, promote the further development of this research field, and open up new directions and paths for the development and practicality of defective MOFs.

DECLARATIONS

Authors' contributions

Conceived the manuscript: Pang H
Wrote the manuscript: Zhang Y
Reviewed the manuscript: Zhang Y, Li Q
Contributed to the discussion of the manuscript: Zhang Y, Li Q, Zhang G, Lv T, Geng P, Chen Y, Pang H

Availability of data and materials

Not applicable.

Financial support and sponsorship

This study was supported by the National Natural Science Foundation of China (NSFC-U1904215), the Natural Science Foundation of Jiangsu Province (BK20200044), and the Program for Young Changjiang Scholars of the Ministry of Education, China (Q2018270). We also acknowledge the Priority Academic Program Development of Jiangsu Higher Education Institutions and the technical support we received at the Testing Center of Yangzhou University.

Conflicts of interest

All authors declared that there are no conflicts of interest.

Ethical approval and consent to participate

Not applicable.

Consent for publication

Not applicable.

REFERENCES

1. Chu S, Majumdar A. Opportunities and challenges for a sustainable energy future. *Nature* 2012;488:294-303. DOI PubMed
2. Elimelech M, Phillip WA. The future of seawater desalination: energy, technology, and the environment. *Science* 2011;333:712-7. DOI PubMed
3. Feng D, Lei T, Lukatskaya MR, et al. Robust and conductive two-dimensional metal-organic frameworks with exceptionally high volumetric and areal capacitance. *Nat Energy* 2018;3:30-6. DOI
4. Guo X, Xu H, Li W, et al. Embedding atomically dispersed iron sites in nitrogen-doped carbon frameworks-wrapped silicon suboxide for superior lithium storage. *Adv Sci* 2023;10:e2206084. DOI PubMed PMC

5. Wu Y, Li Y, Gao J, Zhang Q. Recent advances in vacancy engineering of metal-organic frameworks and their derivatives for electrocatalysis. *SusMat* 2021;1:66-87. DOI
6. Xie J, Wang Z, Xu ZJ, Zhang Q. Toward a high-performance all-plastic full battery with a'single organic polymer as both cathode and anode. *Adv Energy Mater* 2018;8:1703509. DOI
7. Indra A, Song T, Paik U. Metal organic framework derived materials: progress and prospects for the energy conversion and storage. *Adv Mater* 2018;30:e1705146. DOI PubMed
8. Liang HQ, Guo Y, Shi Y, Peng X, Liang B, Chen B. A light-responsive metal-organic framework hybrid membrane with high on/off photoswitchable proton conductivity. *Angew Chem Int Ed* 2020;59:7732-7. DOI
9. Xu Y, Li Q, Xue H, Pang H. Metal-organic frameworks for direct electrochemical applications. *Coord Chem Rev* 2018;376:292-318. DOI
10. Yang H, Wang X. Secondary-component incorporated hollow MOFs and derivatives for catalytic and energy-related applications. *Adv Mater* 2019;31:e1800743. DOI PubMed
11. Zhang G, Jin L, Zhang R, Bai Y, Zhu R, Pang H. Recent advances in the development of electronically and ionically conductive metal-organic frameworks. *Coord Chem Rev* 2021;439:213915. DOI
12. Bediako DK, Surendranath Y, Nocera DG. Mechanistic studies of the oxygen evolution reaction mediated by a nickel-borate thin film electrocatalyst. *J Am Chem Soc* 2013;135:3662-74. DOI PubMed
13. Wei Y, Zheng M, Zhu W, Zhang Y, Hu W, Pang H. Preparation of hierarchical hollow CoFe Prussian blue analogues and its heat-treatment derivatives for the electrocatalyst of oxygen evolution reaction. *J Colloid Interface Sci* 2023;631:8-16. DOI
14. Hang X, Yang R, Xue Y, et al. The introduction of cobalt element into nickel-organic framework for enhanced supercapacitive performance. *Chin Chem Lett* 2023;34:107787. DOI
15. Hang X, Zhao J, Xue Y, Yang R, Pang H. Synergistic effect of Co/Ni bimetallic metal-organic nanostructures for enhanced electrochemical energy storage. *J Colloid Interface Sci* 2022;628:389-96. DOI
16. Wang HF, Chen L, Pang H, Kaskel S, Xu Q. MOF-derived electrocatalysts for oxygen reduction, oxygen evolution and hydrogen evolution reactions. *Chem Soc Rev* 2020;49:1414-48. DOI PubMed
17. Hou CC, Zou L, Wang Y, Xu Q. MOF-mediated fabrication of a porous 3D superstructure of carbon nanosheets decorated with ultrafine cobalt phosphide nanoparticles for efficient electrocatalysis and zinc-air batteries. *Angew Chem Int Ed* 2020;59:21360-6. DOI
18. Liang HW, Zhuang X, Brüller S, Feng X, Müllen K. Hierarchically porous carbons with optimized nitrogen doping as highly active electrocatalysts for oxygen reduction. *Nat Commun* 2014;5:4973. DOI PubMed
19. Wu H, Wang J, Yan J, Wu Z, Jin W. MOF-derived two-dimensional N-doped carbon nanosheets coupled with Co-Fe-P-Se as efficient bifunctional OER/ORR catalysts. *Nanoscale* 2019;11:20144-50. DOI
20. Gong M, Zhou W, Tsai MC, et al. Nanoscale nickel oxide/nickel heterostructures for active hydrogen evolution electrocatalysis. *Nat Commun* 2014;5:4695. DOI
21. Wu X, Jing Q, Sun F, Pang H. The synthesis of zeolitic imidazolate framework/prussian blue analogue heterostructure composites and their application in supercapacitors. *Inorg Chem Front* 2022;10:78-84. DOI
22. Long X, Li G, Wang Z, et al. Metallic iron-nickel sulfide ultrathin nanosheets as a highly active electrocatalyst for hydrogen evolution reaction in acidic media. *J Am Chem Soc* 2015;137:11900-3. DOI
23. Zhong H, Ghorbani-Asl M, Ly KH, et al. Synergistic electroreduction of carbon dioxide to carbon monoxide on bimetallic layered conjugated metal-organic frameworks. *Nat Commun* 2020;11:1409. DOI PubMed PMC
24. Nam DH, Shekhah O, Lee G, et al. Intermediate binding control using metal-organic frameworks enhances electrochemical CO_2 reduction. *J Am Chem Soc* 2020;142:21513-21. DOI
25. Bruce PG, Scrosati B, Tarascon JM. Nanomaterials for rechargeable lithium batteries. *Angew Chem Int Ed* 2008;47:2930-46. DOI PubMed
26. Cheng H, Shapter JG, Li Y, Gao G. Recent progress of advanced anode materials of lithium-ion batteries. *J Energy Chem* 2021;57:451-68. DOI
27. Miao Y, Liu L, Zhang Y, Tan Q, Li J. An overview of global power lithium-ion batteries and associated critical metal recycling. *J Hazard Mater* 2022;425:127900. DOI
28. Sun S, Xie T, Tao S, et al. Formation of nitrogen-doped carbon-coated CoP nanoparticles embedded within graphene oxide for lithium-ion batteries anode. *Energy Technol* 2020;8:1901089. DOI
29. Gao Y, Qiu Z, Lu Y, et al. Rational design and general synthesis of high-entropy metallic ammonium phosphate superstructures assembled by nanosheets. *Inorg Chem* 2023;62:3669-78. DOI
30. Li B, Xue J, Han C, et al. A hafnium oxide-coated dendrite-free zinc anode for rechargeable aqueous zinc-ion batteries. *J Colloid Interface Sci* 2021;599:467-75. DOI
31. Sun F, Chen T, Li Q, Pang H. Hierarchical nickel oxalate superstructure assembled from 1D nanorods for aqueous Nickel-Zinc battery. *J Colloid Interface Sci* 2022;627:483-91. DOI
32. Wang S, Ru Y, Sun Y, Pang H. Fan-like MnV_2O_6 superstructure for rechargeable aqueous zinc ion batteries. *Chin Chem Lett* 2023:108143. DOI
33. Wu L, Dong Y. Recent progress of carbon nanomaterials for high-performance cathodes and anodes in aqueous zinc ion batteries. *Energy Stor Mater* 2021;41:715-37. DOI

34. Elazari R, Salitra G, Garsuch A, Panchenko A, Aurbach D. Sulfur-impregnated activated carbon fiber cloth as a binder-free cathode for rechargeable Li-S batteries. *Adv Mater* 2011;23:5641-4. DOI PubMed
35. Fang D, Wang Y, Qian C, et al. Synergistic regulation of polysulfides conversion and deposition by MOF-derived hierarchically ordered carbonaceous composite for high-energy lithium-sulfur batteries. *Adv Funct Mater* 2019;29:1900875. DOI
36. Li Y, Lin S, Wang D, et al. Single atom array mimic on ultrathin MOF nanosheets boosts the safety and life of lithium-sulfur batteries. *Adv Mater* 2020;32:e1906722. DOI
37. Liu G, Feng K, Cui H, Li J, Liu Y, Wang M. MOF derived in-situ carbon-encapsulated Fe_3O_4@C to mediate polysulfides redox for ultrastable Lithium-sulfur batteries. *Chem Eng J* 2020;381:122652. DOI
38. Luo D, Li C, Zhang Y, et al. Design of quasi-MOF nanospheres as a dynamic electrocatalyst toward accelerated sulfur reduction reaction for high-performance lithium-sulfur batteries. *Adv Mater* 2022;34:e2105541. DOI
39. Yuan N, Sun W, Yang J, Gong X, Liu R. Multifunctional MOF-based separator materials for advanced lithium-sulfur batteries. *Adv Mater Interfaces* 2021;8:2001941. DOI
40. Zhang H, Zhao W, Wu Y, Wang Y, Zou M, Cao A. Dense monolithic MOF and carbon nanotube hybrid with enhanced volumetric and areal capacities for lithium-sulfur battery. *J Mater Chem A* 2019;7:9195-201. DOI
41. Li N, Guo X, Tang X, Xing Y, Pang H. Three-dimensional $Co_2V_2O_7 \cdot nH_2O$ superstructures assembled by nanosheets for electrochemical energy storage. *Chin Chem Lett* 2022;33:462-5. DOI
42. Li P, Bai Y, Zhang G, Guo X, Meng X, Pang H. Surface-halogen-introduced 2D NiCo bimetallic MOFs via a modulation method for elevated electrochemical glucose sensing. *Inorg Chem Front* 2022;9:5853-61. DOI
43. Bi S, Banda H, Chen M, et al. Molecular understanding of charge storage and charging dynamics in supercapacitors with MOF electrodes and ionic liquid electrolytes. *Nat Mater* 2020;19:552-8. DOI
44. Hou S, Lian Y, Bai Y, et al. Hollow dodecahedral Co_3S_4@NiO derived from ZIF-67 for supercapacitor. *Electrochim Acta* 2020;341:136053. DOI
45. Liu C, Bai Y, Li W, Yang F, Zhang G, Pang H. In situ growth of three-dimensional MXene/metal-organic framework composites for high-performance supercapacitors. *Angew Chem Int Ed* 2022;61:e202116282. DOI
46. Sun F, Li Q, Bai Y, et al. A controllable preparation of two-dimensional cobalt oxalate-based nanostructured sheets for electrochemical energy storage. *Chin Chem Lett* 2022;33:3249-54. DOI
47. Lin J, Chenna Krishna Reddy R, Zeng C, Lin X, Zeb A, Su C. Metal-organic frameworks and their derivatives as electrode materials for potassium ion batteries: a review. *Coord Chem Rev* 2021;446:214118. DOI
48. Zhou W, Tang Y, Zhang X, Zhang S, Xue H, Pang H. MOF derived metal oxide composites and their applications in energy storage. *Coord Chem Rev* 2023;477:214949. DOI
49. He B, Zhang Q, Pan Z, et al. Freestanding metal-organic frameworks and their derivatives: an emerging platform for electrochemical energy storage and conversion. *Chem Rev* 2022;122:10087-125. DOI PubMed PMC
50. Li Q, Zhang Y, Zhang G, Wang Y, Pang H. Recent advances in the development of perovskite@metal-organic frameworks composites. *Nat Sci Open* 2023;2:20220065. DOI
51. Carrington EJ, McAnally CA, Fletcher AJ, Thompson SP, Warren M, Brammer L. Solvent-switchable continuous-breathing behaviour in a diamondoid metal-organic framework and its influence on CO_2 versus CH_4 selectivity. *Nat Chem* 2017;9:882-9. DOI
52. Islamoglu T, Goswami S, Li Z, Howarth AJ, Farha OK, Hupp JT. Postsynthetic tuning of metal-organic frameworks for targeted applications. *ACC Chem Res* 2017;50:805-13. DOI PubMed
53. Zhou H, Yang H, Yao S, Jiang L, Sun N, Pang H. Synthesis of 3D printing materials and their electrochemical applications. *Chin Chem Lett* 2022;33:3681-94. DOI
54. Hu Z, Deibert BJ, Li J. Luminescent metal-organic frameworks for chemical sensing and explosive detection. *Chem Soc Rev* 2014;43:5815-40. DOI PubMed
55. Kim KJ, Lu P, Culp JT, Ohodnicki PR. Metal-organic framework thin film coated optical fiber sensors: a novel waveguide-based chemical sensing platform. *ACS Sens* 2018;3:386-94. DOI PubMed
56. Ma WP, Yan B. Lanthanide functionalized MOF thin films as effective luminescent materials and chemical sensors for ammonia. *Dalton Trans* 2020;49:15663-71. DOI PubMed
57. Zhu HL, Huang JR, Liao PQ, Chen XM. Rational design of metal-organic frameworks for electroreduction of CO_2 to hydrocarbons and carbon oxygenates. *ACS Cent Sci* 2022;8:1506-17. DOI PubMed PMC
58. Narváez-celada D, Varela AS. CO_2 electrochemical reduction on metal-organic framework catalysts: current status and future directions. *J Mater Chem A* 2022;10:5899-917. DOI
59. Mohan B, Kumar S, Xi H, et al. Fabricated metal-organic frameworks (MOFs) as luminescent and electrochemical biosensors for cancer biomarkers detection. *Biosens Bioelectron* 2022;197:113738. DOI
60. Zhang L, Qiao C, Cai X, et al. Microcalorimetry-guided pore-microenvironment optimization to improve sensitivity of Ni-MOF electrochemical biosensor for chiral galantamine. *Chem Eng J* 2021;426:130730. DOI
61. Cai G, Yan P, Zhang L, Zhou HC, Jiang HL. Metal-organic framework-based hierarchically porous materials: synthesis and applications. *Chem Rev* 2021;121:12278-326. DOI
62. Chen J, Xiao G, Duan G, Wu Y, Zhao X, Gong X. Structural design of carbon dots/porous materials composites and their applications. *Chem Eng J* 2021;421:127743. DOI
63. Zhou H, Zheng S, Guo X, Gao Y, Li H, Pang H. Ordered porous and uniform electric-field-strength micro-supercapacitors by 3D

printing based on liquid-crystal V_2O_5 nanowires compositing carbon nanomaterials. *J Colloid Interface Sci* 2022;628:24-32. DOI
64. Gao Z, Hsu CH, Liu J, et al. Synthesis and characterization of a single-layer conjugated metal-organic structure featuring a non-trivial topological gap. *Nanoscale* 2019;11:878-81. DOI
65. Mähringer A, Jakowetz AC, Rotter JM, et al. Oriented thin films of electroactive triphenylene catecholate-based two-dimensional metal-organic frameworks. *ACS Nano* 2019;13:6711-9. DOI
66. Zheng S, Zhou H, Xue H, Braunstein P, Pang H. Pillared-layer Ni-MOF nanosheets anchored on Ti_3C_2 MXene for enhanced electrochemical energy storage. *J Colloid Interface Sci* 2022;614:130-7. DOI PubMed
67. Qutaish H, Lee J, Hyeon Y, et al. Design of cobalt catalysed carbon nanotubes in bimetallic zeolitic imidazolate frameworks. *Appl Surf Sci* 2021;547:149134. DOI
68. Xie LS, Skorupskii G, Dincă M. Electrically conductive metal-organic frameworks. *Chem Rev* 2020;120:8536-80. DOI PubMed PMC
69. Pang Q, Yang L, Li Q. Vacancies in metal-organic frameworks: formation, arrangement, and functions. *Small Struct* 2022;3:2100203. DOI
70. Batten SR, Robson R. Interpenetrating nets: ordered, periodic entanglement. *Angew Chem Int Ed* 1998;37:1460-94. PubMed
71. Ren J, Ledwaba M, Musyoka NM, et al. Structural defects in metal-organic frameworks (MOFs): formation, detection and control towards practices of interests. *Coord Chem Rev* 2017;349:169-97. DOI
72. Taddei M. When defects turn into virtues: the curious case of zirconium-based metal-organic frameworks. *Coord Chem Rev* 2017;343:1-24. DOI
73. Liu L, Chen Z, Wang J, et al. Imaging defects and their evolution in a metal-organic framework at sub-unit-cell resolution. *Nat Chem* 2019;11:622-8. DOI
74. Fang Z, Bueken B, De Vos DE, Fischer RA. Defect-engineered metal-organic frameworks. *Angew Chem Int Ed* 2015;54:7234-54. DOI PubMed PMC
75. Xiang W, Zhang Y, Chen Y, Liu C, Tu X. Synthesis, characterization and application of defective metal-organic frameworks: current status and perspectives. *J Mater Chem A* 2020;8:21526-46. DOI
76. Dissegna S, Epp K, Heinz WR, Kieslich G, Fischer RA. Defective metal-organic frameworks. *Adv Mater* 2018;30:e1704501. DOI PubMed
77. Piao Y, Meany B, Powell LR, et al. Brightening of carbon nanotube photoluminescence through the incorporation of sp3 defects. *Nat Chem* 2013;5:840-5. DOI
78. Tuller HL, Bishop SR. Point defects in oxides: tailoring materials through defect engineering. *Annu Rev Mater Res* 2011;41:369-98. DOI
79. Slater B, Wang Z, Jiang S, Hill MR, Ladewig BP. Missing linker defects in a homochiral metal-organic framework: tuning the chiral separation capacity. *J Am Chem Soc* 2017;139:18322-7. DOI
80. Wu H, Chua YS, Krungleviciute V, et al. Unusual and highly tunable missing-linker defects in zirconium metal-organic framework UiO-66 and their important effects on gas adsorption. *J Am Chem Soc* 2013;135:10525-32. DOI
81. Vos A, Hendrickx K, Van Der Voort P, Van Speybroeck V, Lejaeghere K. Missing linkers: an alternative pathway to UiO-66 electronic structure engineering. *Chem Mater* 2017;29:3006-19. DOI PubMed PMC
82. Yuan S, Zou L, Qin JS, et al. Construction of hierarchically porous metal-organic frameworks through linker labilization. *Nat Commun* 2017;8:15356. DOI PubMed PMC
83. Xue Z, Liu K, Liu Q, et al. Missing-linker metal-organic frameworks for oxygen evolution reaction. *Nat Commun* 2019;10:5048. DOI PubMed PMC
84. Liu QQ, Liu SS, Liu XF, et al. Superprotonic conductivity of UiO-66 with missing-linker defects in aqua-ammonia vapor. *Inorg Chem* 2022;61:3406-11. DOI
85. Basu O, Mukhopadhyay S, Laha S, Das SK. Defect engineering in a metal-organic framework system to achieve super-protonic conductivity. *Chem Mater* 2022;34:6734-43. DOI
86. Rowsell JL, Yaghi OM. Metal-organic frameworks: a new class of porous materials. *Microporous Mesoporous Mater* 2004;73:3-14. DOI
87. Idrees KB, Chen Z, Zhang X, et al. Tailoring pore aperture and structural defects in zirconium-based metal-organic frameworks for krypton/xenon separation. *Chem Mater* 2020;32:3776-82. DOI
88. Chammingkwan P, Shangkum GY, Mai LTT, et al. Modulator-free approach towards missing-cluster defect formation in Zr-based UiO-66. *RSC Adv* 2020;10:28180-5. DOI PubMed PMC
89. Ma X, Wang L, Zhang Q, Jiang H. Switching on the photocatalysis of metal-organic frameworks by engineering structural defects. *Angew Chem Int Ed* 2019;131:12303-7. DOI PubMed
90. Fei H, Shin J, Meng YS, et al. Reusable oxidation catalysis using metal-monocatecholato species in a robust metal-organic framework. *J Am Chem Soc* 2014;136:4965-73. DOI
91. Nickerl G, Senkovska I, Kaskel S. Tetrazine functionalized zirconium MOF as an optical sensor for oxidizing gases. *Chem Commun* 2015;51:2280-2. DOI PubMed
92. Pullen S, Fei H, Orthaber A, Cohen SM, Ott S. Enhanced photochemical hydrogen production by a molecular diiron catalyst incorporated into a metal-organic framework. *J Am Chem Soc* 2013;135:16997-7003. DOI PubMed PMC
93. Cliffe MJ, Wan W, Zou X, et al. Correlated defect nanoregions in a metal-organic framework. *Nat Commun* 2014;5:4176. DOI

PubMed PMC

94. Taddei M, Wakeham RJ, Koutsianos A, Andreoli E, Barron AR. Post-synthetic ligand exchange in zirconium-based metal-organic frameworks: beware of the defects! *Angew Chem Int Ed* 2018;57:11706-10. DOI PubMed
95. Shearer GC, Chavan S, Bordiga S, Svelle S, Olsbye U, Lillerud KP. Defect engineering: tuning the porosity and composition of the metal-organic framework UiO-66 via modulated synthesis. *Chem Mater* 2016;28:3749-61. DOI
96. Gao W, Li X, Zhang X, et al. Photocatalytic nitrogen fixation of metal-organic frameworks (MOFs) excited by ultraviolet light: insights into the nitrogen fixation mechanism of missing metal cluster or linker defects. *Nanoscale* 2021;13:7801-9. DOI
97. Barin G, Krungleviciute V, Gutov O, Hupp JT, Yildirim T, Farha OK. Defect creation by linker fragmentation in metal-organic frameworks and its effects on gas uptake properties. *Inorg Chem* 2014;53:6914-9. DOI PubMed
98. Pang Q, Tu B, Yang L, Li Q. Photochemical cycloaddition and temperature-dependent breathing in pillared-layer metal-organic frameworks. *Sci Bull* 2019;64:1881-9. DOI
99. Zhang W, Kauer M, Guo P, et al. Impact of synthesis parameters on the formation of defects in HKUST-1. *Eur J Inorg Chem* 2017;2017:925-31. DOI
100. He S, Chen Y, Zhang Z, Ni B, He W, Wang X. Competitive coordination strategy for the synthesis of hierarchical-pore metal-organic framework nanostructures. *Chem Sci* 2016;7:7101-5. DOI PubMed PMC
101. Koo J, Hwang IC, Yu X, Saha S, Kim Y, Kim K. Hollowing out MOFs: hierarchical micro- and mesoporous MOFs with tailorable porosity via selective acid etching. *Chem Sci* 2017;8:6799-803. DOI PubMed PMC
102. Yang J, Chen X, Li Y, Zhuang Q, Liu P, Gu J. Zr-based MOFs shielded with phospholipid bilayers: improved biostability and cell uptake for biological applications. *Chem Mater* 2017;29:4580-9. DOI
103. Wang Z, Hu S, Yang J, et al. Nanoscale Zr-based MOFs with tailorable size and introduced mesopore for protein delivery. *Adv Funct Mater* 2018;28:1707356. DOI
104. Choi KM, Jeon HJ, Kang JK, Yaghi OM. Heterogeneity within order in crystals of a porous metal-organic framework. *J Am Chem Soc* 2011;133:11920-3. DOI PubMed
105. Cai G, Jiang HL. A modulator-induced defect-formation strategy to hierarchically porous metal-organic frameworks with high stability. *Angew Chem Int Ed* 2017;56:563-7. DOI PubMed
106. Dissegna S, Epp K, Heinz WR, Kieslich G, Fischer RA. Metal-organic frameworks: defective metal-organic frameworks. *Adv Mater* 2018;30:1870280. DOI
107. Forgan RS. Modulated self-assembly of metal-organic frameworks. *Chem Sci* 2020;11:4546-62. DOI PubMed PMC
108. Liu B, Vellingiri K, Jo S, Kumar P, Ok YS, Kim K. Recent advances in controlled modification of the size and morphology of metal-organic frameworks. *Nano Res* 2018;11:4441-67. DOI
109. Winarta J, Shan B, Mcintyre SM, et al. A decade of UiO-66 research: a historic review of dynamic structure, synthesis mechanisms, and characterization techniques of an archetypal metal-organic framework. *Cryst Growth Des* 2020;20:1347-62. DOI
110. Shan B, Mcintyre SM, Armstrong MR, Shen Y, Mu B. Investigation of missing-cluster defects in UiO-66 and ferrocene deposition into defect-induced cavities. *Ind Eng Chem Res* 2018;57:14233-41. DOI
111. Iacomi P, Formalik F, Marreiros J, et al. Role of structural defects in the adsorption and separation of C3 hydrocarbons in Zr-fumarate-MOF (MOF-801). *Chem Mater* 2019;31:8413-23. DOI
112. Ye G, Gu Y, Zhou W, Xu W, Sun Y. Synthesis of defect-rich titanium terephthalate with the assistance of acetic acid for room-temperature oxidative desulfurization of fuel oil. *ACS Catal* 2020;10:2384-94. DOI
113. Zhang H, Shi R, Fan H, et al. Defect creation by benzoic acid in Cu-based metal-organic frameworks for enhancing sulfur capture. *Microporous Mesoporous Mater* 2020;298:110070. DOI
114. Wang J, Liu L, Chen C, et al. Engineering effective structural defects of metal-organic frameworks to enhance their catalytic performances. *J Mater Chem A* 2020;8:4464-72. DOI
115. Lázaro I, Wells CJR, Forgan RS. Multivariate modulation of the Zr MOF UiO-66 for defect-controlled combination anticancer drug delivery. *Angew Chem Int Ed* 2020;132:5249-55. DOI PubMed PMC
116. Gutov OV, Molina S, Escudero-Adán EC, Shafir A. Modulation by amino acids: toward superior control in the synthesis of zirconium metal-organic frameworks. *Chemistry* 2016;22:13582-7. DOI PubMed
117. Assaad N, Sabeh G, Hmadeh M. Defect control in Zr-based metal-organic framework nanoparticles for arsenic removal from water. *ACS Appl Nano Mater* 2020;3:8997-9008. DOI
118. Jiang J, Lu Z, Zhang M, et al. Higher symmetry multinuclear clusters of metal-organic frameworks for highly selective CO_2 capture. *J Am Chem Soc* 2018;140:17825-9. DOI
119. Muldoon PF, Liu C, Miller CC, et al. Programmable topology in new families of heterobimetallic metal-organic frameworks. *J Am Chem Soc* 2018;140:6194-8. DOI
120. Kang X, Lyu K, Li L, et al. Integration of mesopores and crystal defects in metal-organic frameworks via templated electrosynthesis. *Nat Commun* 2019;10:4466. DOI PubMed PMC
121. Kim S, Kim A, Yoon JW, Kim H, Bae Y. Creation of mesoporous defects in a microporous metal-organic framework by an acetic acid-fragmented linker co-assembly and its remarkable effects on methane uptake. *Chem Eng J* 2018;335:94-100. DOI
122. Liu X, Qi W, Wang Y, Su R, He Z. A facile strategy for enzyme immobilization with highly stable hierarchically porous metal-organic frameworks. *Nanoscale* 2017;9:17561-70. DOI
123. Xu R, Ji Q, Zhao P, et al. Hierarchically porous UiO-66 with tunable mesopores and oxygen vacancies for enhanced arsenic removal.

J Mater Chem A 2020;8:7870-9. DOI

124. Xu W, Thapa KB, Ju Q, Fang Z, Huang W. Heterogeneous catalysts based on mesoporous metal-organic frameworks. *Coord Chem Rev* 2018;373:199-232. DOI
125. Bunck DN, Dichtel WR. Mixed linker strategies for organic framework functionalization. *Chemistry* 2013;19:818-27. DOI PubMed
126. Kozachuk O, Luz I, Llabrés i Xamena FX, et al. Multifunctional, defect-engineered metal-organic frameworks with ruthenium centers: sorption and catalytic properties. *Angew Chem Int Ed* 2014;53:7058-62. DOI
127. Yuan S, Qin JS, Zou L, et al. Thermodynamically guided synthesis of mixed-linker Zr-MOFs with enhanced tunability. *J Am Chem Soc* 2016;138:6636-42. DOI
128. Bueken B, Van Velthoven N, Krajnc A, et al. Tackling the defect conundrum in UiO-66: a mixed-linker approach to engineering missing linker defects. *Chem Mater* 2017;29:10478-86. DOI
129. Deng H, Doonan CJ, Furukawa H, et al. Multiple functional groups of varying ratios in metal-organic frameworks. *Science* 2010;327:846-50. DOI
130. Jrad A, Hmadeh M, Awada G, Chakleh R, Ahmad M. Efficient biofuel production by MTV-UiO-66 based catalysts. *Chem Eng J* 2021;410:128237. DOI
131. Chaemchuen S, Luo Z, Zhou K, et al. Defect formation in metal-organic frameworks initiated by the crystal growth-rate and effect on catalytic performance. *J Catal* 2017;354:84-91. DOI
132. Chu L, Guo J, Wang L, et al. Synthesis of defected UIO-66 with boosting the catalytic performance via rapid crystallization. *Appl Organomet Chem* 2021;36:e6559. DOI
133. Feng X, Hajek J, Jena HS, et al. Engineering a highly defective stable UiO-66 with tunable lewis- brønsted acidity: the role of the hemilabile linker. *J Am Chem Soc* 2020;142:3174-83. DOI
134. Yang P, Mao F, Li Y, Zhuang Q, Gu J. Hierarchical porous Zr-based MOFs synthesized by a facile monocarboxylic acid etching strategy. *Chemistry* 2018;24:2962-70. DOI PubMed
135. Gadipelli S, Guo Z. Postsynthesis annealing of MOF-5 remarkably enhances the framework structural stability and CO_2 uptake. *Chem Mater* 2014;26:6333-8. DOI
136. Pan T, Shen Y, Wu P, et al. Thermal shrinkage behavior of metal-organic frameworks. *Adv Funct Mater* 2020;30:2001389. DOI
137. Shearier E, Cheng P, Bao J, Hu YH, Zhao F. Surface defection reduces cytotoxicity of Zn(2-methylimidazole)$_2$ (ZIF-8) without compromising its drug delivery capacity. *RSC Adv* 2016;6:4128-35. DOI PubMed PMC
138. Steenhaut T, Grégoire N, Barozzino-Consiglio G, Filinchuk Y, Hermans S. Mechanochemical defect engineering of HKUST-1 and impact of the resulting defects on carbon dioxide sorption and catalytic cyclopropanation. *RSC Adv* 2020;10:19822-31. DOI PubMed PMC
139. Avci C, Ariñez-soriano J, Carné-sánchez A, et al. Post-synthetic anisotropic wet-chemical etching of colloidal sodalite ZIF crystals. *Angew Chem Int Ed* 2015;127:14625-9. DOI
140. Liang Y, Li C, Chen L, et al. Microwave-assisted acid-induced formation of linker vacancies within Zr-based metal organic frameworks with enhanced heterogeneous catalysis. *Chin Chem Lett* 2021;32:787-90. DOI
141. Doan HV, Sartbaeva A, Eloi JC, Davis SA, Ting VP. Defective hierarchical porous copper-based metal-organic frameworks synthesised via facile acid etching strategy. *Sci Rep* 2019;9:10887. DOI PubMed PMC
142. Albolkany MK, Liu C, Wang Y, et al. Molecular surgery at microporous MOF for mesopore generation and renovation. *Angew Chem Int Ed* 2021;60:14601-8. DOI
143. Chang GG, Ma XC, Zhang YX, et al. Construction of hierarchical metal-organic frameworks by competitive coordination strategy for highly efficient CO_2 conversion. *Adv Mater* 2019;31:e1904969. DOI
144. Zhang B, Qi Z, Wu Z, et al. Defect-rich 2D material networks for advanced oxygen evolution catalysts. *ACS Energy Lett* 2019;4:328-36. DOI
145. Meng F, Zhang S, Ma L, et al. Construction of hierarchically porous nanoparticles@metal-organic frameworks composites by inherent defects for the enhancement of catalytic efficiency. *Adv Mater* 2018;30:e1803263. DOI
146. Jia M, Mai L, Li Z, Li W. Air-thermal processing of hierarchically porous metal-organic frameworks. *Nanoscale* 2020;12:14171-9. DOI
147. Bennett TD, Todorova TK, Baxter EF, et al. Connecting defects and amorphization in UiO-66 and MIL-140 metal-organic frameworks: a combined experimental and computational study. *Phys Chem Chem Phys* 2016;18:2192-201. DOI
148. Cheng P, Hu YH. Acetylene adsorption on defected MIL-53. *Int J Energy Res* 2016;40:846-52. DOI
149. Geng P, Wang L, Du M, et al. MIL-96-Al for Li-S batteries: shape or size? *Adv Mater* 2022;34:e2107836. DOI
150. Masoomi MY, Morsali A, Dhakshinamoorthy A, Garcia H. Mixed-metal MOFs: unique opportunities in metal-organic framework (MOF) functionality and design. *Angew Chem Int Ed* 2019;131:15330-47. DOI PubMed
151. Peng Y, Bai Y, Liu C, Cao S, Kong Q, Pang H. Applications of metal-organic framework-derived N, P, S doped materials in electrochemical energy conversion and storage. *Coord Chem Rev* 2022;466:214602. DOI
152. Wang Y, Zhao L, Ma J, Zhang J. Confined interface transformation of metal-organic frameworks for highly efficient oxygen evolution reactions. *Energy Environ Sci* 2022;15:3830-41. DOI
153. Svane KL, Bristow JK, Gale JD, Walsh A. Vacancy defect configurations in the metal-organic framework UiO-66: energetics and electronic structure. *J Mater Chem A* 2018;6:8507-13. DOI PubMed PMC
154. Zhao X, Pattengale B, Fan D, et al. Mixed-node metal-organic frameworks as efficient electrocatalysts for oxygen evolution reaction.

ACS Energy Lett 2018;3:2520-6. DOI

155. Cao Y, Li P, Wu T, Liu M, Zhang Y. Electrocatalysis of N_2 to NH_3 by HKUST-1 with High NH_3 Yield. *Chem Asian J* 2020;15:1272-6. DOI
156. Li J, Zhang W, Zhang X, et al. Copolymer derived micro/meso-porous carbon nanofibers with vacancy-type defects for high-performance supercapacitors. *J Mater Chem A* 2020;8:2463-71. DOI
157. Lázaro IA, Szalad H, Valiente P, Albero J, García H, Martí-Gastaldo C. Tuning the photocatalytic activity of Ti-based metal-organic frameworks through modulator defect-engineered functionalization. *ACS Appl Mater Interfaces* 2022;14:21007-17. DOI PubMed PMC
158. Li S, Wang H, Wulan B, Zhang X, Yan J, Jiang Q. Complete dehydrogenation of $N_2H_4BH_3$ over noble-metal-free $Ni_{0.5}Fe_{0.5}$-CeO_x/MIL-101 with high activity and 100% H_2 selectivity. *Adv Energy Mater* 2018;8:1800625. DOI
159. Yang R, Peng S, Lan B, et al. Oxygen defect engineering of β-MnO_2 catalysts via phase transformation for selective catalytic reduction of NO. *Small* 2021;17:e2102408. DOI
160. Dhakshinamoorthy A, Li Z, Garcia H. Catalysis and photocatalysis by metal organic frameworks. *Chem Soc Rev* 2018;47:8134-72. DOI PubMed
161. Liu S, Teng Z, Liu H, et al. A Ce-UiO-66 metal-organic framework-based graphene-embedded photocatalyst with controllable activation for solar ammonia fertilizer production. *Angew Chem Int Ed* 2022;61:e202207026. DOI
162. Wang S, Wang X, Cheng X, Ma J, Sun W. Tailoring defect-type and ligand-vacancies in Zr(iv) frameworks for CO_2 photoreduction. *J Mater Chem A* 2022;10:16396-402. DOI
163. Li G, Blake GR, Palstra TT. Vacancies in functional materials for clean energy storage and harvesting: the perfect imperfection. *Chem Soc Rev* 2017;46:1693-706. DOI PubMed
164. Jiang D, Zhu Y, Chen M, et al. Modified crystal structure and improved photocatalytic activity of MIL-53 via inorganic acid modulator. *Appl Catal B Environ* 2019;255:117746. DOI
165. Hao YC, Chen LW, Li J, et al. Metal-organic framework membranes with single-atomic centers for photocatalytic CO_2 and O_2 reduction. *Nat Commun* 2021;12:2682. DOI PubMed PMC
166. Seh ZW, Kibsgaard J, Dickens CF, Chorkendorff I, Nørskov JK, Jaramillo TF. Combining theory and experiment in electrocatalysis: insights into materials design. *Science* 2017;355:eaad4998. DOI PubMed
167. Zhao S, Wang Y, Dong J, et al. Ultrathin metal-organic framework nanosheets for electrocatalytic oxygen evolution. *Nat Energy* 2016;1:16184. DOI
168. Tahir M, Pan L, Idrees F, et al. Electrocatalytic oxygen evolution reaction for energy conversion and storage: a comprehensive review. *Nano Energy* 2017;37:136-57. DOI
169. Zhang L, Jia Y, Gao G, et al. Graphene defects trap atomic Ni species for hydrogen and oxygen evolution reactions. *Chem* 2018;4:285-97. DOI
170. Hod I, Deria P, Bury W, et al. A porous proton-relaying metal-organic framework material that accelerates electrochemical hydrogen evolution. *Nat Commun* 2015;6:8304. DOI PubMed PMC
171. Su X, Wang Y, Zhou J, Gu S, Li J, Zhang S. Operando spectroscopic identification of active sites in NiFe prussian blue analogues as electrocatalysts: activation of oxygen atoms for oxygen evolution reaction. *J Am Chem Soc* 2018;140:11286-92. DOI
172. Xu H, Cao J, Shan C, et al. MOF-derived hollow CoS decorated with CeO_x nanoparticles for boosting oxygen evolution reaction electrocatalysis. *Angew Chem Int Ed* 2018;130:8790-4. DOI
173. Zou Z, Wang J, Pan H, et al. Enhanced oxygen evolution reaction of defective CoP/MOF-integrated electrocatalyst by partial phosphating. *J Mater Chem A* 2020;8:14099-105. DOI
174. Zhao S, Tan C, He C, et al. Structural transformation of highly active metal-organic framework electrocatalysts during the oxygen evolution reaction. *Nat Energy* 2020;5:881-90. DOI
175. Kang T, Kim J. Optimal cobalt-based catalyst containing high-ratio of oxygen vacancy synthesized from metal-organic-framework (MOF) for oxygen evolution reaction (OER) enhancement. *Appl Surf Sci* 2021;560:150035. DOI
176. Chen X, Wang Z, Wei Y, et al. High phase-purity 1T-MoS_2 ultrathin nanosheets by a spatially confined template. *Angew Chem Int Ed* 2019;58:17621-4. DOI
177. Han A, Zhou X, Wang X, et al. One-step synthesis of single-site vanadium substitution in 1T-WS_2 monolayers for enhanced hydrogen evolution catalysis. *Nat Commun* 2021;12:709. DOI PubMed PMC
178. Sokolikova MS, Sherrell PC, Palczynski P, Bemmer VL, Mattevi C. Direct solution-phase synthesis of 1T' WSe_2 nanosheets. *Nat Commun* 2019;10:712. DOI PubMed PMC
179. Rui K, Zhao G, Lao M, et al. Direct hybridization of noble metal nanostructures on 2D metal-organic framework nanosheets to catalyze hydrogen evolution. *Nano Lett* 2019;19:8447-53. DOI
180. Wang D, Li Q, Han C, Lu Q, Xing Z, Yang X. Atomic and electronic modulation of self-supported nickel-vanadium layered double hydroxide to accelerate water splitting kinetics. *Nat Commun* 2019;10:3899. DOI PubMed PMC
181. Sun H, Chen L, Lian Y, et al. Topotactically transformed polygonal mesopores on ternary layered double hydroxides exposing under-coordinated metal centers for accelerated water dissociation. *Adv Mater* 2020;32:e2006784. DOI
182. Gopi S, Panda A, Ramu A, Theerthagiri J, Kim H, Yun K. Bifunctional electrocatalysts for water splitting from a bimetallic (V doped-NixFey) metal-organic framework MOF@Graphene oxide composite. *Int J Hydrog Energy* 2022;47:42122-35. DOI
183. Fu J, Cano ZP, Park MG, Yu A, Fowler M, Chen Z. Electrically rechargeable zinc-air batteries: progress, challenges, and

perspectives. *Adv Mater* 2017;29:1604685. DOI PubMed
184. Stamenkovic VR, Strmcnik D, Lopes PP, Markovic NM. Energy and fuels from electrochemical interfaces. *Nat Mater* 2016;16:57-69. DOI PubMed
185. Wang XX, Swihart MT, Wu G. Achievements, challenges and perspectives on cathode catalysts in proton exchange membrane fuel cells for transportation. *Nat Catal* 2019;2:578-89. DOI
186. Lin L, Zhou W, Gao R, et al. Low-temperature hydrogen production from water and methanol using Pt/α-MoC catalysts. *Nature* 2017;544:80-3. DOI
187. Qiao B, Wang A, Yang X, et al. Single-atom catalysis of CO oxidation using Pt_1/FeO_x. *Nat Chem* 2011;3:634-41. DOI
188. Yuan S, Zhang J, Hu L, et al. Decarboxylation-induced defects in MOF-derived single cobalt Atom@Carbon electrocatalysts for efficient oxygen reduction. *Angew Chem Int Ed* 2021;60:21685-90. DOI
189. Wu Q, Jia Y, Liu Q, et al. Ultra-dense carbon defects as highly active sites for oxygen reduction catalysis. *Chem* 2022;8:2715-33. DOI
190. Chen X, Pu J, Hu X, An L, Jiang J, Li Y. Confinement synthesis of bimetallic MOF-derived defect-rich nanofiber electrocatalysts for rechargeable Zn-air battery. *Nano Res* 2022;15:9000-9. DOI
191. Li J, Xia W, Tang J, et al. Metal-organic framework-derived graphene mesh: a robust scaffold for highly exposed Fe-N_4 active sites toward an excellent oxygen reduction catalyst in acid media. *J Am Chem Soc* 2022;144:9280-91. DOI
192. Ling LL, Jiao L, Liu X, et al. Potassium-assisted fabrication of intrinsic defects in porous carbons for electrocatalytic CO_2 reduction. *Adv Mater* 2022;34:e2205933. DOI
193. Hu C, Wang Y, Chen J, et al. Main-Group metal single-atomic regulators in dual-metal catalysts for enhanced electrochemical CO_2 reduction. *Small* 2022;18:e2201391. DOI
194. Kang X, Li L, Sheveleva A, et al. Electro-reduction of carbon dioxide at low over-potential at a metal-organic framework decorated cathode. *Nat Commun* 2020;11:5464. DOI PubMed PMC
195. Albo J, Perfecto-Irigaray M, Beobide G, Irabien A. Cu/Bi metal-organic framework-based systems for an enhanced electrochemical transformation of CO_2 to alcohols. *J CO2 Util* 2019;33:157-65. DOI
196. Albo J, Vallejo D, Beobide G, Castillo O, Castaño P, Irabien A. Copper-based metal-organic porous materials for CO_2 electrocatalytic reduction to alcohols. *ChemSusChem* 2017;10:1100-9. DOI PubMed
197. Ye G, Zhang D, Li X, et al. Boosting catalytic performance of metal-organic framework by increasing the defects via a facile and green approach. *ACS Appl Mater Interfaces* 2017;9:34937-43. DOI
198. Xu W, Zhang Y, Wang J, et al. Defects engineering simultaneously enhances activity and recyclability of MOFs in selective hydrogenation of biomass. *Nat Commun* 2022;13:2068. DOI PubMed PMC
199. Feng L, Day GS, Wang K, Yuan S, Zhou H. Strategies for pore engineering in zirconium metal-organic frameworks. *Chem* 2020;6:2902-23. DOI
200. Li J, Bhatt PM, Li J, Eddaoudi M, Liu Y. Recent progress on microfine design of metal-organic frameworks: structure regulation and gas sorption and separation. *Adv Mater* 2020;32:e2002563. DOI PubMed
201. Yilmaz G, Peh SB, Zhao D, Ho GW. Atomic- and molecular-level design of functional metal-organic frameworks (MOFs) and derivatives for energy and environmental applications. *Adv Sci* 2019;6:1901129. DOI PubMed PMC
202. Feng Y, Cao X, Zhang L, et al. Defect engineering of enzyme-embedded metal-organic frameworks for smart cargo release. *Chem Eng J* 2022;439:135736. DOI
203. Sun D, Wong LW, Wong HY, et al. Direct visualization of atomic structure in multivariate metal-organic frameworks (MOFs) for guiding electrocatalysts design. *Angew Chem Int Ed* 2023;135:e202216008. DOI
204. Huang Y, Jiao Y, Chen T, et al. Tuning the wettability of metal-organic frameworks via defect engineering for efficient oil/water separation. *ACS Appl Mater Interfaces* 2020;12:34413-22. DOI
205. Li Y, Zhang J, Chen Q, Xia X, Chen M. Emerging of heterostructure materials in energy storage: a review. *Adv Mater* 2021;33:e2100855. DOI
206. Liu J, Song X, Zhang T, Liu S, Wen H, Chen L. 2D conductive metal-organic frameworks: an emerging platform for electrochemical energy storage. *Angew Chem Int Ed* 2021;133:5672-84. DOI
207. Li Q, Li S, Sha J, et al. $NiMo_6$/ZIF-67 nanostructures on graphitic carbon nitride for colorimetric sensing of hydrogen peroxide and ascorbic acid. *ACS Appl Nano Mater* 2021;4:12197-203. DOI
208. Li Q, Xu M, Wang T, Wang H, Sun J, Sha J. Nanohybridization of CoS_2/MoS_2 heterostructure with polyoxometalate on functionalized reduced graphene oxide for high-performance LIBs. *Chemistry* 2022;28:e202200207. DOI
209. Liu J, Kopold P, van Aken PA, Maier J, Yu Y. Energy storage materials from nature through nanotechnology: a sustainable route from reed plants to a silicon anode for lithium-ion batteries. *Angew Chem Int Ed* 2015;127:9768-72. DOI
210. Maier J. Thermodynamics of electrochemical lithium storage. *Angew Chem Int Ed* 2013;52:4998-5026. DOI PubMed
211. Cheng F, Liang J, Tao Z, Chen J. Functional materials for rechargeable batteries. *Adv Mater* 2011;23:1695-715. DOI
212. Dunn B, Kamath H, Tarascon JM. Electrical energy storage for the grid: a battery of choices. *Science* 2011;334:928-35. DOI PubMed
213. Dou S, Tao L, Wang R, El Hankari S, Chen R, Wang S. Plasma-assisted synthesis and surface modification of electrode materials for renewable energy. *Adv Mater* 2018;30:e1705850. DOI PubMed
214. Sun S, Chen D, Shen M, et al. Plasma modulated MOF-derived TiO_2/C for enhanced lithium storage. *Chem Eng J* 2021;417:128003.

DOI

215. Lin J, Huang T, Lu M, Lin X, Reddy RCK, Xu X. Modulating electronic structure of metal-organic frameworks derived zinc manganates by oxygen vacancies for superior lithium storage. *Chem Eng J* 2022;433:133770. DOI
216. Lv T, Zhu G, Dong S, et al. Co-intercalation of dual charge carriers in metal-ion-confining layered vanadium oxide nanobelts for aqueous zinc-ion batteries. *Angew Chem Int Ed* 2023;62:e202216089. DOI
217. Nian Q, Zhang X, Feng Y, et al. Designing electrolyte structure to suppress hydrogen evolution reaction in aqueous batteries. *ACS Energy Lett* 2021;6:2174-80. DOI
218. Sun T, Zhang W, Nian Q, Tao Z. Proton-insertion dominated polymer cathode for high-performance aqueous zinc-ion battery. *Chem Eng J* 2023;452:139324. DOI
219. Li P, Ren J, Li C, et al. MOF-derived defect-rich CeO_2 as ion-selective smart artificial SEI for dendrite-free Zn-ion battery. *Chem Eng J* 2023;451:138769. DOI
220. Leng W, Cui L, Liu Y, Gong Y. MOF-derived MnV_2O_4/C microparticles with graphene coating anchored on graphite sheets: oxygen defect engaged high performance aqueous zinc-ion battery. *Adv Mater Interfaces* 2022;9:2101705. DOI
221. Sun K, Pang J, Zheng Y, et al. Oxygen vacancies enriched MOF-derived MnO/C hybrids for high-performance aqueous zinc ion battery. *J Alloys Compd* 2022;923:166470. DOI
222. Du M, Geng P, Pei C, et al. High-entropy prussian blue analogues and their oxide family as sulfur hosts for lithium-sulfur batteries. *Angew Chem Int Ed* 2022;61:e202209350. DOI
223. Wang N, Zhang X, Ju Z, et al. Thickness-independent scalable high-performance Li-S batteries with high areal sulfur loading via electron-enriched carbon framework. *Nat Commun* 2021;12:4519. DOI PubMed PMC
224. Yang Y, Zheng G, Cui Y. Nanostructured sulfur cathodes. *Chem Soc Rev* 2013;42:3018-32. DOI PubMed
225. Manthiram A, Fu Y, Chung SH, Zu C, Su YS. Rechargeable lithium-sulfur batteries. *Chem Rev* 2014;114:11751-87. DOI PubMed
226. Wei Seh Z, Li W, Cha JJ, et al. Sulphur-TiO_2 yolk-shell nanoarchitecture with internal void space for long-cycle lithium-sulphur batteries. *Nat Commun* 2013;4:1331. DOI
227. Liu M, Zhang C, Su J, et al. Propelling polysulfide conversion by defect-rich MoS_2 nanosheets for high-performance lithium-sulfur batteries. *ACS Appl Mater Interfaces* 2019;11:20788-95. DOI
228. Wang Y, Zhang R, Chen J, et al. Enhancing catalytic activity of titanium oxide in lithium-sulfur batteries by band engineering. *Adv Energy Mater* 2019;9:1900953. DOI
229. He Q, Yu B, Wang H, Rana M, Liao X, Zhao Y. Oxygen defects boost polysulfides immobilization and catalytic conversion: first-principles computational characterization and experimental design. *Nano Res* 2020;13:2299-307. DOI
230. Li S, Lin J, Ding Y, et al. Defects engineering of lightweight metal-organic frameworks-based electrocatalytic membrane for high-loading lithium-sulfur batteries. *ACS Nano* 2021;15:13803-13. DOI
231. Zhang X, Li G, Zhang Y, et al. Amorphizing metal-organic framework towards multifunctional polysulfide barrier for high-performance lithium-sulfur batteries. *Nano Energy* 2021;86:106094. DOI
232. Wang X, Zhao C, Liu B, et al. Creating edge sites within the 2D metal-organic framework boosts redox kinetics in lithium-sulfur batteries. *Adv Energy Mater* 2022;12:2201960. DOI
233. Jiang Y, Deng YP, Liang R, et al. D-orbital steered active sites through ligand editing on heterometal imidazole frameworks for rechargeable zinc-air battery. *Nat Commun* 2020;11:5858. DOI PubMed PMC
234. Liu R, Xu S, Shao X, et al. Defect-engineered NiCo-S composite as a bifunctional electrode for high-performance supercapacitor and electrocatalysis. *ACS Appl Mater Interfaces* 2021;13:47717-27. DOI
235. Wang H, Yin F, Liu N, Yu H, Fan T, Chen B. Engineering mesopores and unsaturated coordination in metal-organic frameworks for enhanced oxygen reduction and oxygen evolution activity and Li-air battery capacity. *ACS Sustain Chem Eng* 2021;9:4509-19. DOI